iScience

CellPress
OPEN ACCESS

Article

New AAV9 engineered variants with enhanced neurotropism and reduced liver off-targeting in mice and marmosets

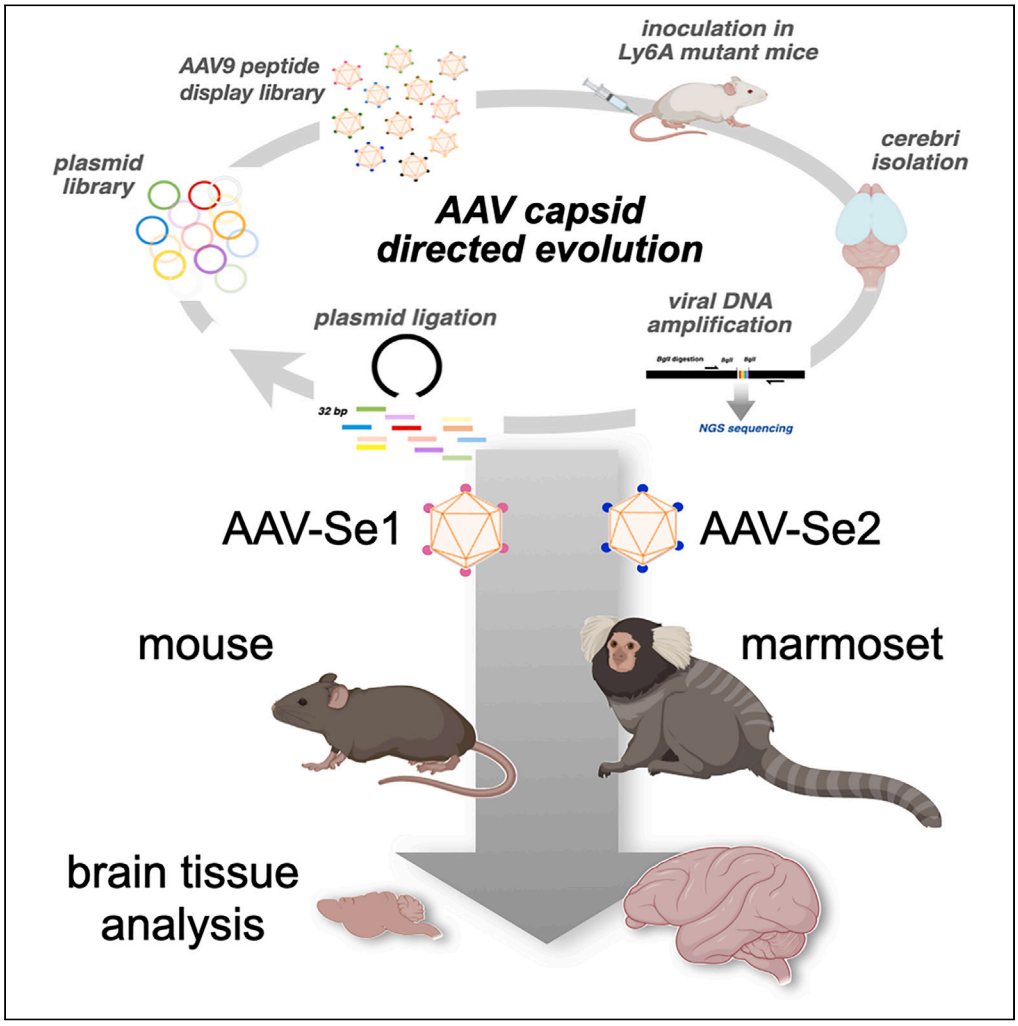

Serena Gea Giannelli, Mirko Luoni, Angelo Iannielli, ..., Simone Bido, Jakob Körbelin, Vania Broccoli

broccoli.vania@hsr.it

Highlights

AAV-Se1/2 are novel neurotropic AAV9 display peptide modified capsids

AAV-Se1/2 have high brain tropism in adult mice and marmosets

Inactivation of the galactose-binding domain erases AAV9 tissue off-targeting

AAV-Se2 partially depends on the Ly6C1 and Ly6E receptors

Giannelli et al., iScience 27, 109777
May 17, 2024
https://doi.org/10.1016/j.isci.2024.109777

iScience

CellPress
OPEN ACCESS

Article

New AAV9 engineered variants with enhanced neurotropism and reduced liver off-targeting in mice and marmosets

Serena Gea Giannelli,[1,5] Mirko Luoni,[1,2,5] Angelo Iannielli,[1,2] Jinte Middeldorp,[3] Ingrid Philippens,[3] Simone Bido,[1] Jakob Körbelin,[4] and Vania Broccoli[1,2,6,*]

SUMMARY

Although adeno-associated virus 9 (AAV9) has been highly exploited as delivery platform for gene-based therapies, its efficacy is hampered by low efficiency in crossing the adult blood-brain barrier (BBB) and pronounced targeting to the liver upon intravenous delivery. We generated a new galactose binding-deficient AAV9 peptide display library and selected two new AAV9 engineered capsids with enhanced targeting in mouse and marmoset brains after intravenous delivery. Interestingly, the loss of galactose binding greatly reduced undesired targeting to peripheral organs, particularly the liver, while not compromising transduction of the brain vasculature. However, the galactose binding was necessary to efficiently infect non-endothelial brain cells. Thus, the combinatorial actions of the galactose-binding domain and the incorporated displayed peptide are crucial to enhance BBB crossing along with brain cell transduction. This study describes two novel capsids with high brain endothelial infectivity and extremely low liver targeting based on manipulating the AAV9 galactose-binding domain.

INTRODUCTION

Adeno-associated virus (AAV) vectors are the most commonly used delivery system for *in vivo* gene therapy in preclinical and clinical studies.[1–6] AAV vectors consist of a protein capsid that shields a single-stranded DNA genome and determines the vector tropism. Natural serotypes offer a suite of delivery platforms with multiple opportunities for tissue and organ targeting.[7–9] However, most of them have a pronounced tropism to the liver when administered intravenously, limiting transduction efficiency in other organs and raising important concerns of toxicity.[10–12] The definition of the AAV capsid structure at high resolution and identification of their cellular receptors and intracellular pathways have provided the necessary knowledge to introduce targeted modifications aimed at reconfiguring the viral behavior *in vivo*, such as tissue tropism, stability, or immunity.[13,14] To this end, several AAV library-based approaches have been elaborated to isolate new variants with the desired property through an iterative selection *in vitro* or *in vivo* known as directed evolution. This strategy has proven to be very powerful, yielding engineered capsids with compelling new or improved properties. Various modalities have been exploited for rational capsid engineering, notably single amino acid substitutions, capsid chimeras by DNA shuffling, or the targeted insertion of random peptides into key positions that control capsid-cell receptor interactions, an approach referred to as random peptide display.[15–17] The latter strategy was pioneered by two German groups who implanted a random 7-amino acid sequence into positions R588 and N587 of AAV2-VP1 to introduce high-sequence diversity on superficial domains of the capsid to maximize the engagement with new cell receptors.[18,19] Importantly, this domain is primarily responsible for the binding of AAV2 to its natural receptor heparan sulfate.[20] In fact, the integration of the peptide reduced heparin binding by at least 70% compared to the unmodified AAV2.[18] Thus, this strategy, on the one side, significantly reduced the natural binding of AAV2 and on the other side surveyed new interactions through the display of a random sequence. This design, coupled with multiple rounds of capsid selection *in vivo*, enabled for the isolation of variants with superior tropism compared to the parental AAV2 for coronary artery, pulmonary and brain endothelial cells,[18,21,22] lung,[23] liver,[24] and cardiomyocytes,[25] among others. With the same rationale, a random heptapeptide sequence was inserted into the AAV9 capsid at position A589, corresponding to the analogue domain of the AAV2 capsid.[26,27] However, unlike AAV2, this domain is not responsible for AAV9 binding to galactose, its natural primary cell receptor.[28–30] Thus, this peptide display system diversifies an important domain on the surface of the AAV9 capsid, but its interactions should complement or counteract the binding specificity dictated by the galactose engagement that still remains in place. Using an analogous library equipped with a Cre-dependent

[1]Division of Neuroscience, IRCCS San Raffaele Scientific Institute, 20132 Milan, Italy
[2]CNR Institute of Neuroscience, 20854 Vedano al Lambro, Italy
[3]Biomedical Primate Research Centre (BPRC), 2288 GJ Rijswijk, the Netherlands
[4]Department of Oncology, Hematology and Bone Marrow Transplantation, University Medical Center Hamburg-Eppendorf, 20246 Hamburg, Germany
[5]These authors contributed equally
[6]Lead contact
*Correspondence: broccoli.vania@hsr.it
https://doi.org/10.1016/j.isci.2024.109777

selectable cassette, the PHP.B viral family was isolated with a superior ability to cross the BBB and transduce the central and peripheral nervous systems.[31,32] However, this behavior is not conserved in other mammals, as their transduction was found to be dependent on the binding to the rodent-specific endothelial Ly6A receptor.[33–36] Remarkably, *in vivo* selection of AAV9 peptide display libraries also led to the identification of RGD motif-containing capsids with a superior efficiency and selectivity for muscle tissue after intravenous injection in mice and non-human primates (NHPs).[37,38] Thus, AAV engineered libraries coupled with effective selection strategies have provided an invaluable system for isolating new capsids with selected traits tailored for specific applications. Herein, we generated a new display library using the AAV9 galactose-binding mutant capsid to abrogate its natural tropism and redirect it to alternative cell receptors. Iterative *in vivo* selection for superior neurotropic viruses after intravenous administration identified two novel variants that outperformed the parental natural capsid and maintained high transduction efficiencies in both C57BL/6 and BALB/c mice. In addition, both engineered capsids showed superior gene transfer capability in adult marmosets and human neuronal cultures with compared to the unmodified AAV9. Interestingly, we showed that the lack of galactose binding suppressed off-target transduction in the liver without compromising the targeting to the brain vasculature.

RESULTS

Generation and screening of a new AAV9 peptide display library

In order to maximize the targeting diversity of the AAV9, we reasoned that removing the galactose binding capability of the capsid would facilitate the identification of new interactions between the random display peptides and their cellular targets. The AAV9 capsid contains a small galactose binding pocket and point mutations in this domain reduce its binding compromising its transduction efficiency in tissues.[28–30] We introduced the W503A mutation which was described to virtually eliminate the galactose binding and prevent the viral transduction in cells.[30] Then, we inserted a randomized sequence of 7 amino acids (7-mer) between amino acids 588 and 589 of the mutant W503A VP1 variant (Figure 1A). Based on the cloning strategy two additional amino acids, a glycine and alanine, were flanking the random sequence. We speculated that given their small hindrance and neutral charge, these amino acids would not represent a significant impediment to the binding, but rather enhance the flexibility of the loop created by the random sequence. The diversity of the produced plasmid library was 1×10^8 clones per library as assessed by targeted deep-sequencing. Next, we transferred the plasmid library into AAV producing cells with a minimal amount of plasmid per cell to minimize that multiple plasmids would be incorporated into single producer cells with the high risk to produce chimeric capsids. Sequencing of infected clones indicated that the diversity of the viral library was comparable to that of the plasmid library ensuring an efficient and unbiased production of the AAV library.

We, next, sought to exploit this library to identify new AAV9 variants acquiring the ability to cross the BBB in adult BALB/c mice. This mouse strain has proven to be resistant to brain transduction by the PHP.B family of capsids since their putative receptor Ly6A is mutated and not exposed to the cell membrane.[33–36] Thus, these mice offered a convenient and straightforward system to prevent the selection of Ly6A-binding capsids to begin with. A single dose of 2×10^{11} vector genomes (vg) of the display peptide library was injected into the tail vein of BALB/c adult mice (Figure 1B). Three weeks after viral inoculation, the brain was isolated, cerebral cortices dissected and lysed to harvest the DNA of the viral particles that successfully homed into the brain (Figure 1B). The relevant part of the capsid gene was amplified by PCR, re-cloned into a new library, and the selection process was then repeated for three additional rounds (Figure 1B). After each round, deep-sequencing of the viral DNA amplicon was performed to trace the progressive enrichment of viral sequences with preferential targeting to the brain tissue (Figure 1B). After the first two rounds of selection, 5 out of the 7 residues had strongly enriched one specific amino acid (Figure S1). After the third round the most represented peptide was NGVRSVG (13% of total reads), however a new, and clearly distinct, motif became apparent to the following and last cycle, with the sequence PGVPGRF (34% of total reads) (Figures 1C and 1D). We named the two new variants as AAV-A503-Se1 and AAV-A503-Se2 in the order they appeared during the different rounds of selection. The presence of the W503A mutation did not alter significantly the yield of viral production of either the library or the selected variants.

Brain transduction pattern of AAV-A503-Se1 and AAV-A503-Se2 in C57BL/6 and BALB/c mice

We generated a reporter vector containing the ZsGreen, which ensures a brighter fluorescence compared to GFP, under the control of the CBA promoter and packaged it into the AAV-A503-Se1 and AAV-A503-Se2 capsids (Figure 2A). In addition, we generated an AAV9-A503 mutant capsid as a pertinent negative control. For immunofluorescence analysis, we validated two antibodies against ZsGreen raised in different host species which provided specific and comparable results on brain sections (Figure S2). C57BL/6 mice injected with the AAV9 capsid mutant at the dose of 1×10^{11} vg/mouse failed to show ZsGreen staining in the brain confirming a loss of transduction as expected (Figure 2B). Conversely, both AAV-A503-Se1/2 capsid variants at the same dose sustained a diffuse transgene expression throughout the brain (Figure 2B). Importantly, ZsGreen expression was comparable in both C57BL/6 and BALB/c strains of mice for both capsid variants suggesting that their transduction was independent from the PHP.B receptor Ly6A (Figure 2B). In particular, we noted that mice treated with either capsid variant showed intense ZsGreen fluorescence in the vasculature throughout the cortices (Figure 2B). Double immunofluorescence staining between the ZsGreen and the endothelial-specific marker CD31 (Pecam1) showed over 80% of productive viral transduction of endothelial cells throughout the brain for both AAV-Se variants. In contrast, only a minority of $CD31^-$ cells, all together below 8%, in the brain parenchyma expressed the viral transgene with either variant in any of the two mouse strains (Figures 2C–2E). Consistent with previous results, viral genome quantifications by qPCR revealed a 12- and 16-fold increase from brain lysates transduced with AAV-A503-Se1 and -Se2, respectively, compared to AAV9-A503 (Figure 2F). These findings indicate that the AAV-A503-Se variants acquired the ability to efficiently target the brain by transducing mostly its vasculature while being highly inefficient to infect other brain cells.

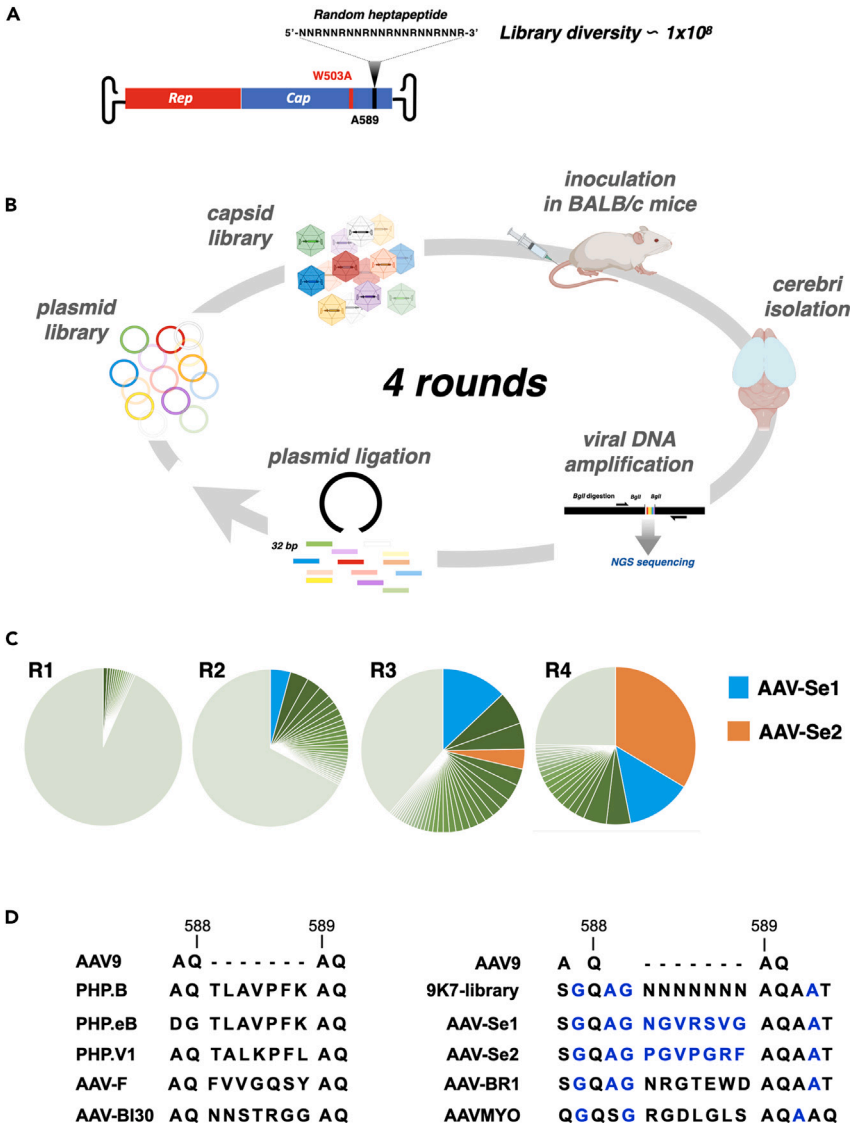

Figure 1. Outline of AAV9 peptide display library selection procedure and NGS sequencing results

(A) Illustration of AAV9 construct indicating the distinctive features of our library: the W503A mutation in the *Cap* cistron that amperes galactose binding and the position A589 where the heptapeptide display library was inserted. The heptapeptide library was encoded by a 21nt, whose codons in the third position presents only with a G or an A (R).

(B) Illustration of the main procedures undertaken during each round of library screening, focusing on the brain cortex as main target tissue.

(C) Pie charts indicate the frequency of each different 7mer sequences determined by NGS. In the brain, the highest ranking 7mer at the 3rd round (R3) was named AAV-Se1 (Blue), which upon a 4th round (R4) was overcome by another variant, named AAV-Se2 (Orange).

(D) AAV-Se1 and -Se2 heptamers and contiguous residues are compared to the parental library sequence, native AAV9, as well as various other AAV9- (PHP.B, PHP.eB, PHP.V1, AAV-F and CAP-B130) and AAV2- (AAV-BR1) based capsid variants.

High and diffuse brain transduction of AAV-Se1/2 capsid variants by restoring the galactose binding capability

We reasoned that a possible explanation for the lack of the AAV-A503-Se capsids to transduce brain cells beyond the vasculature was their inability to bind galactose. To assess if this was the case, we reverted the Alanine into Tryptophan in position 503 of AAV-VP1 in both AAV-Se capsids to restore their capacity to bind to galactose (Figure 3A). We then packaged a single-stranded ZsGreen-expressing vector into both capsids and administrated a viral dose of 1×10^{11} vg to adult mice by intravenous injections. As reference controls, we produced AAV9 and AAV-PHP.eB viruses packaging the equivalent reporter and inoculated in mice as executed for the AAV-Se capsids. Three weeks post-transduction, ZsGreen distribution was assessed within the brains in both C57BL/6 and BALB/c mice. Interestingly, wild-type AAV-Se1/2 showed a significantly more diffuse tropism in the brain respect to their mutant analogues and the unmodified AAV9 (Figure 3B). Although the general level of distribution of the AAV-Se1/2 viruses appeared comparable to that of PHP.eB in C57BL/6 mice, their pattern of infection in BALB/c

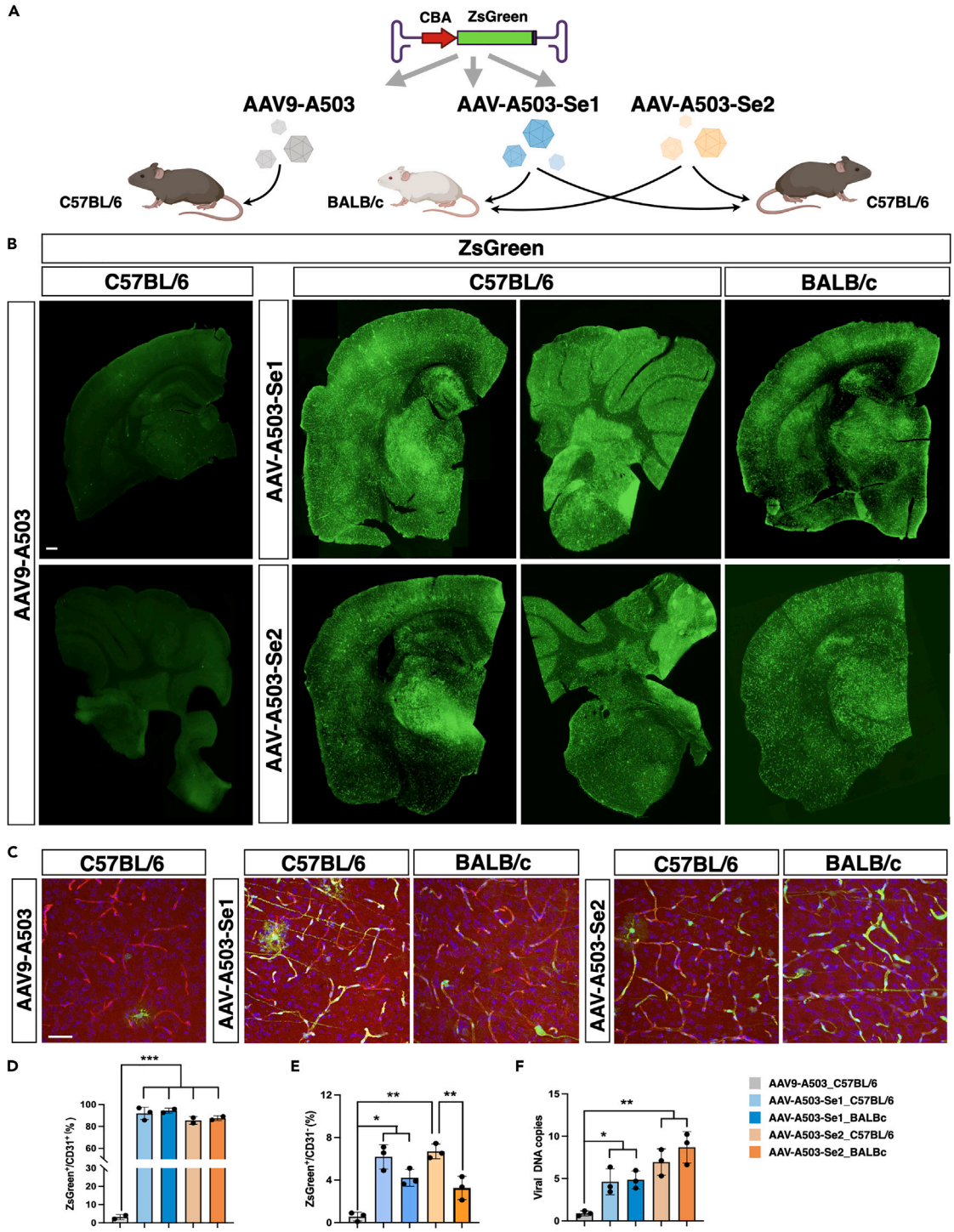

Figure 2. AAV-A503-Se1 and AAV-A503-Se2 exhibit a high brain tropism selectively for endothelial cells in both C57BL/6 and BALB/c mice

(A) Illustration of the experimental setting. Wild-type C57BL/6 and BALB/c mice are systemically injected with AAV9-A503, AAV-A503-Se1 and AAV-A503-Se2 carrying the ZsGreen transgene under the control of the CBA strong constitutive promoter (experimental viral dose: 1×10^{11} vg/mouse, $n = 3$ animals for each group).

(B) Low magnification immunostaining for ZsGreen, in cerebrum and cerebellum derived from animals treated with AAV9-A503, AAV-A503-Se1 and AAV-A503-Se2. Scale bar, 200 μm.

(C) High magnification immunostaining for ZsGreen and CD31 (in red) in cortex derived from animals treated with AAV9-A503, AAV-A503-Se1 and AAV-A503-Se2. Scale bar, 100 μm.

Figure 2. *Continued*

(D) Quantitative assessment of virally transduced (ZsGreen$^+$) endothelial cells (CD31$^+$) in brain derived from AAV9-A503, AAV-A503-Se1 and AAV-A503-Se2 treated C57BL/6 and BALB/c mice (n = 3 animals per group, 3 field per mice).

(E) Percentage of non-endothelial cells (CD31$^-$) transduced by the AAV-A503-Se1 and AAV-A503-Se2 in C57BL/6 and BALB/c mice (n = 3 animals per group, 3 field per mice).

(F) Viral DNA vector quantification by qRT-PCR in cortexes derived from AAV9-A503, AAV-A503-Se1 and AAV-A503-Se2 treated C57BL/6 and BALB/c mice. The results are reported as the fold change of viral ZsGreen DNA in mice treated with AAV-A503-Se1 and AAV-A503-Se2 relative to mice treated with AAV9-A503 (n = 3 animals per group). Values are mean ± SD. *p < 0.05; **p < 0.01, ***p < 0.001. Statistical analysis is performed using one-way ANOVA followed by Tukey post-test.

mice did not differ significantly from that of PHP.eB (Figure 3B). Viral genome qPCR quantifications from brain lysates confirmed a substantial comparable transduction efficiency of AAV-Se1/2 in both mouse strains, which resulted highly superior to that of standard AAV9 and not significantly different from the gene transfer levels reached by AAV-PHP.eB (Figure 3C). To determine the identity of the brain cells transduced by AAV-Se1/2, we performed immunohistochemistry for specific markers of neurons (NeuN), astrocytes (Sox9) and endothelial cells (CD31), three weeks after intravenous transduction of adult C57BL/6 and BALB/c mice (Figure 4). Wild-type AAV-Se1 maintained a tropism mainly selective for CD31$^+$ brain endothelial cells in both mouse strains (92% ± 3% in C57BL/6 and 86% ± 3% in BALB/c). Non-endothelial cells infected by AAV-Se1 were very rare and predominantly astrocytes in the brain parenchyma (0.4% ± 0.1% and 0.2% ± 0.05% of NeuN$^+$ neurons in C57BL/6 and BALB/c, respectively; 0.7% ± 0.2% and 0.6% ± 0.3% of Sox9$^+$ astrocytes in C57BL/6 and BALB/c, respectively) (Figure 4). In contrast, wild-type AAV-Se2-mediated transgene expression was found more broadly in the brain parenchyma. In fact, AAV-Se2 gene transfer in brain cells was significantly more efficient with respect to the parental AAV9. AAV-Se2 sustained an increased transduction of neuronal and glial cells compared to the AAV9 by a factor of 7 and 5, respectively (Figure 4). Of note, AAV-Se2 targeted more astrocytes (42.38% ± 5.73%) than PHP.eB (34.21% ± 4.25%), and the reverse was true for neurons (19.67% ± 4.2% for AAV-Se2 and 38.29% ± 3.16% for PHP.eB), suggestive of a slightly different tropism between those two capsids in C57BL/6 mice (Figure 4). In contrast, Olig2$^+$ oligodendrocytes were poorly infected by both AAV-Se1/2, matching the levels of the parental AAV9 (0.18% ± 0.15% for AAV-Se1; 0.55% ± 0.12% for AAV-Se1; 0.31% ± 0.26% for AAV-Se1) (Figure S3A). Interestingly, IBA1$^+$ cortical microglial cells exhibited a well-ramified morphology characteristic of the resting state after infection with any capsids and the signal intensity remain unaltered, suggesting that viral transduction did not cause a persistent and long-term neuroinflammation state (Figure S4A). No appreciable region-to-region variation was observed in AAV-Se1/2-mediated gene transfer in terms of cell type specificity and total infection rate suggesting a consistent and homogeneous transduction profile across the entire brain. Finally, we compared the infectivity rates of the parental AAV9 with its capsid variants on primary mouse neuronal cultures in the dish (Figure S5). Interestingly, wild-type AAV-Se1/Se2 showed a significantly higher transduction efficiency on 10 days *in vitro* mouse primary neuronal cultures compared to both PHP.eB and unmodified AAV9 showed (AAV9 39% ± 1.8%; PHP.eB, 38% ± 3%; AAV-Se1, 88% ± 3%; AAV-Se2 81% ± 6% of Map2$^+$ neurons) (Figure S5). Conversely, the A503 mutant capsids were incompetent to gene transfer, with the exception of the AAV-A503-Se1 which sustained a diffuse infection although with reduced levels of ZsGreen expression (AAV-A502-Se1, 42% ± 1.5% of Map2$^+$ neurons) (Figure S5).

Distribution of AAV-Se1/2 viruses in peripheral organs after systemic delivery

In the fourth round of our original directed-evolution screening, we isolated a number of peripheral organs (liver, lung, heart, spleen, kidney, muscle), beyond the brain, and performed deep-sequencing of the viral amplicons to profile the off-target transduction propensity of the selected capsid variants. Interestingly, while the AAV-Se1 showed an enrichment in most of these organs, the AAV-Se2 was much less represented (Figure 5A). Next, we isolated the livers from C57BL/6 mice transduced with the AAV-Se1/2 and parental AAV9 viruses with or without the A503 mutation and expressing the ZsGreen expressing cassette, at the dose of 1×10^{11} vg/mouse. ZsGreen expression was barely detectable in livers transduced with the A503-mutant AAV9 and AAV-Se1/2 capsids indicating a general minimal tropism of these mutant viruses for this organ (Figure 5B). In addition, viral DNA copy quantifications revealed an even further reduced transduction capability of the AAV-A503-Se capsids, especially AAV-A503-Se2, compared to the parental AAV9 for the liver (Figure 5C). Correction of the A503 mutation in the AAV9 capsid enables to regain high tropism for the liver after intravenous administration in adult mice (Figure 5B). However, even the wild-type AAV-Se1/2 capsids maintained a significant reduced transduction rate in the liver compared to the parental capsid with 3- and 8-fold reduction for the AAV-Se1 and AAV-Se2, respectively (Figures 5B and 5C).

Analysis of AAV-Se1/2 brain tropisms in adult marmosets and human neurons

We next sought to determine whether AAV-Se1/2 conserved a higher brain transduction efficiency respect to the unmodified AAV9 in NHPs. To this end, a single dose (3×10^{13} vg) of AAV9, AAV-Se1 or -Se2, expressing the ZsGreen reporter, was injected into the femoral vein of adult marmosets previously selected for lacking any inherent immune response to AAV capsids. 3 weeks after viral administration the brains and peripheral organs were isolated and sections and lysates were prepared for immunohistochemistry and viral copy quantification, respectively (Figure 6A). During this time no adverse behavioral effects were observed in the treated animals with no gross changes in weight (Table S1). Additionally, liver enzyme levels and blood cell counts were normal at the time of sacrifice indicating the complete lack of enduring liver or systemic organic sufferance caused by either the surgery or the viral-based transgene expression (Table S2). ZsGreen staining on immunodecorated forebrain and cerebellar sections was homogeneously more intense after delivery with AAV-Se1 or -Se2 compared to AAV9

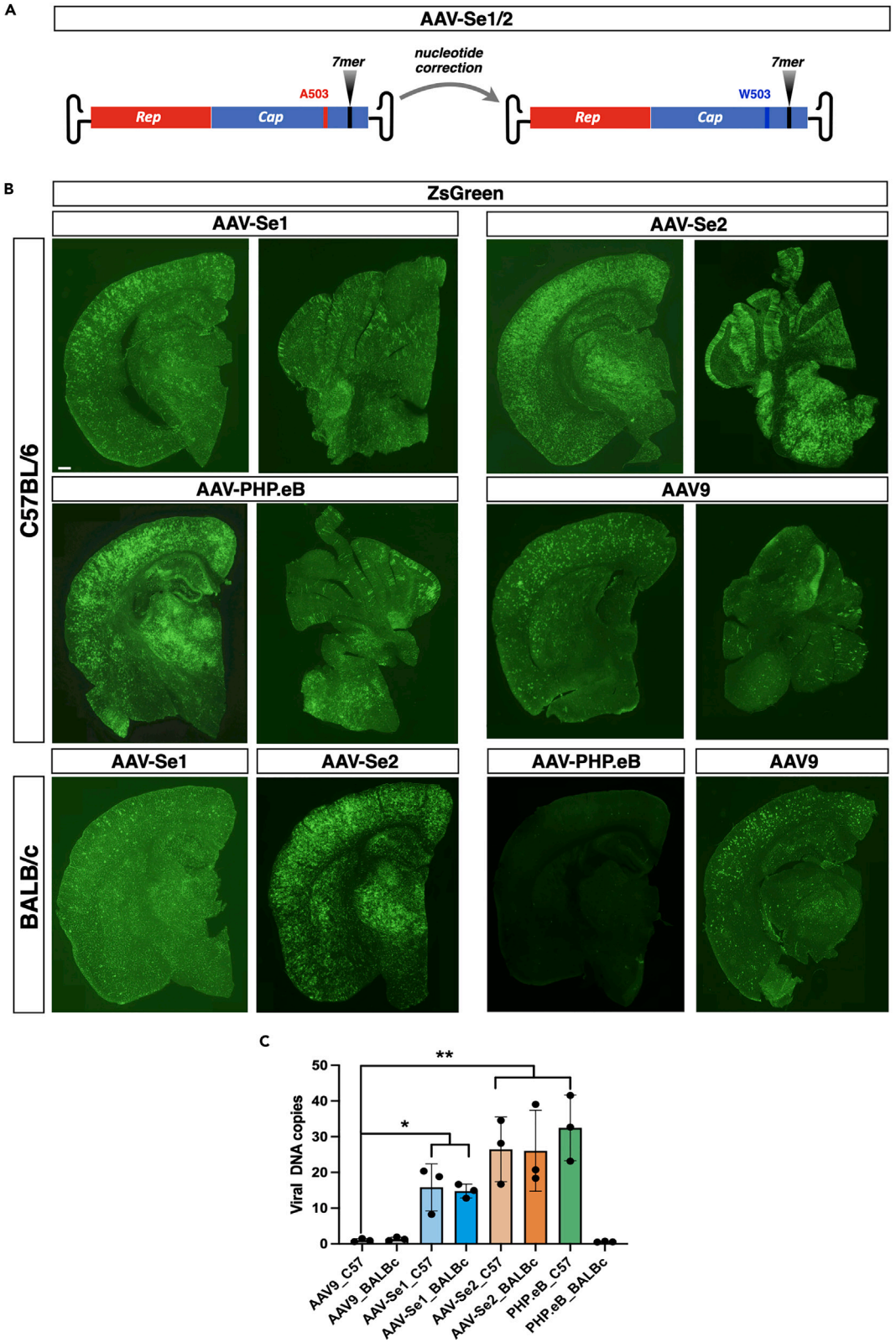
A
AAV-Se1/2
7mer
nucleotide correction
7mer
A503
W503
Rep
Cap
Rep
Cap
B
ZsGreen
AAV-Se1
AAV-Se2
C57BL/6
AAV-PHP.eB
AAV9
AAV-Se1
AAV-Se2
AAV-PHP.eB
AAV9
BALB/c
C
Viral DNA copies
50
40
30
20
10
0
**
*
AAV9_C57
AAV9_BALBc
AAV-Se1_C57
AAV-Se1_BALBc
AAV-Se2_C57
AAV-Se2_BALBc
PHP.eB_C57
PHP.eB_BALBc

Figure 3. Restoring galactose binding reinforces the AAV-Se1/2 infectivity in both C57BL/6 and BALB/c mice

(A) Graphical illustration of the restoration of the galactose binding (A503W amino acid change).

(B) Low magnification immunostaining for ZsGreen in cerebrum and cerebellum derived from animals treated with AAV9, AAV-PHP.eB, AAV-Se1 and AAV-Se2. Scale bars, 200 μm.

(C) Viral DNA vector quantification by qRT-PCR and (D) fold change differences of ZsGreen mRNA levels in cortices in cortices derived from AAV9, AAV-PHP.eB, AAV-Se1 and AAV-Se2 treated C57BL/6 and BALB/c mice. The results are reported as fold change of viral ZsGreen DNA in mice treated with AAV-PHP.eB, AAV-Se1, AAV-Se2 relative to mice treated with AAV9 ($n = 3$ animals per group). Values are mean ± SD. *$p < 0.05$, **$p < 0.01$. Statistical analysis is performed using one-way ANOVA followed by Tukey post-test.

(Figure 6B). Likewise, the mRNA levels of the reporter were significantly higher respect to the AAV9 both in the cortex and cerebellum (2.2 ± 0.4 and 4.2 ± 0.9 for the cortex; 3.6 ± 0.8 and 4.7 ± 1.5 for the cerebellum for AAV-se1 and AAV-Se2, respectively) (Figure 6C). Of note, the numbers of cerebellar Purkinje cells infected with AAV-Se1/2 were significantly increased compared to that with AAV9 as revealed by Calbindin and ZsGreen co-staining (9% ± 3%, 14% ± 2%; 26% ± 5% of Calbindin$^+$ Purkinje cells for AAV9, AAV-Se2 and AAV-Se1, respectively) (Figure 6D). Wide brain distribution of ZsGreen was visualized by DAB-mediated immunostaining in case of the AAV-Se2 showing overall homogeneous staining throughout the brain which was localized in cells with both neuronal, glial and endothelial morphology and with a relative enhanced transduction in the caudoputamen and thalamus (Figures 6E and S6A). Interestingly, quantification of DNA vector copy number indicated that AAV-Se1/2 compared to the parental AAV9 were endowed with higher transduction in the cerebral cortex and cerebellum but had a significantly reduced tropism for the peripheral organs such as liver, muscle and heart (Figure S6B). To assess the cell-type specific transduction mediated by the AAV-Se1/2, we performed co-staining between the NeuN neuronal or Sox9 glial specific markers and the viral reporter ZsGreen. Interestingly, both AAV-Se1/2 sustained significantly higher transductions in neurons and astrocytes compared to AAV9 on cortical sections of the infected brains (AAV9: 1% ± 0.4% MAP2$^+$ neurons, 3% ± 1% Sox9$^+$ astrocytes; AAV-Se1: 2.5% ± 0.8% MAP2$^+$ neurons, 7% ± 2% Sox9$^+$ astrocytes; AAV-Se2: 6% ± 2% MAP2$^+$ neurons, 9% ± 3% Sox9$^+$ astrocytes) (Figures S6C and S6D). Conversely, Olig2$^+$ oligodendrocytes were equally poorly transduced by AAV-Se1/2 and AAV9 (Figure S3B). Morphology and the signal intensity of IBA1$^+$ microglial cells were consistent with the resting state in cortices infected with the different capsids, suggesting that the viral transduction did not elicit long-term inflammatory cues (Figure S4B).

To determine whether AAV-Se1/2 could also transduce human neurons, we tested them in human neuronal cultures differentiated from induced pluripotent stem cells (iPSCs). 6-weeks old iPSC-derived cortical neuronal cultures were infected with ZsGreen expressing AAV-Se1/2 or relative control viruses including PHP.eB, wild-type and A503 mutant AAV9 (Figure 7A). Interestingly, AAV-Se1/2 and PHP.eB exhibited comparable levels of infectivity of MAP2$^+$ neurons that were significantly higher to that of wild-type AAV9 (AAV-Se2 41% ± 4%, AAV-Se1 36% ± 3%, PHP.eB 29% ± 4%, AAV9 21% ± 3%) (Figure 7A). In contrast the mutant AAV9 failed to support gene transfer in human neurons indicating that galactose binding is an absolute requirement for the AAV9 capsid to transduce neurons *in vitro*.

AAV-Se1/2 viruses showed different dependence by the Ly6c1/2 receptors

Next, we sought to confirm that the AAV-Se1/2-mediated transduction was independent by the PHP.B receptor Ly6A. For this goal, we expressed Ly6a in HeLa cells, since giving their human origin they do not express it endogenously and assessed whether this *in vitro* setting was sufficient to discriminate the PHP.eB dependence by Ly6A. In fact, PHP.eB showed a marked increase in infectivity only when HeLa cells expressed its receptor Ly6A (Figure 7B). Encouraged by this result, AAV-Se1 and -Se2 were used to infect HeLa cells expressing or not Ly6a, but both cell cultures resulted poorly susceptible to AAV-Se1/Se2, suggesting that Ly6A did not confer any advantage for AAV-Se1/Se2 transduction (Figure 7B). Ly6A is one member of the Ly6 family of GPI-anchored proteins highly expressed in the endothelium.[33–36] However, among the different Ly6 homologues, the Ly6c1 protein shares a similar enrichment in brain endothelial cells (Figure 7C). Thus, we sought to test whether AAV-Se1 and -Se2 showed any dependence on Ly6c1 or its highly homologue protein Ly6c2 for cell transduction. Remarkably, while gene transfer efficiency was not changed with AAV-Se1, we scored a significant increase in AAV-Se2-mediated expression in both Ly6c1- and Ly6c2-expressing cells. These results clearly suggested that AAV-Se2, but not AAV-Se1, infectivity is at least partly mediated by both Ly6c1 and Lyc2 receptors. Moreover, we quantified transduction efficiency by ZsGreen fluorescence flow cytometry (Figures 7D and S7). From this analysis, it is noticeable that basal PHP.eB infectivity was minimal in HeLa cells not expressing any GPI protein (2.8% of total cells), as well as AAV9 (6.7% of total cells) whereas it was much higher for AAV-Se2 (17.2% of total cells) and even more for AAV-Se1 (49.5% of total cells). Thus, some levels of infectivity of the AAV-Se capsids can occur in HeLa cells in basal conditions, suggesting additional viral/cell interactions which sustain successful gene transfer. Ly6E is another homolog receptor of the family with high expression in brain endothelial cells and conserved in all mammalian species.[32,33] Thus, we generated LY6E deficient HeLa cells by introducing a homozygous indel mutation by CRISPR/Cas9 technology (Figure S7). Interestingly, AAV-Se2, but not AAV-Se1, showed a reduced infectivity in Ly6E mutant HeLa cells (Figure S8). Thus, these results suggest that successful AAV-Se2 transduction is mainly dependent by the LyC1/2 receptors, but LY6E can yet sustain a residual infectivity of this AAV variant possibly acting as an alternative low-affinity receptor. Moreover, the presence of the W503A mutation was detrimental for cell transduction that dropped of 130, 62, and 70 times for AAV9, AAV-Se1, and AAV-Se2, respectively. No ZsGreen$^+$ cells were detectable in HeLa cells infected with PHP.eB-A503 (Figure S8). Interestingly the mutant counterpart maintained, although reduced, their dependency on specific GPI protein (Figure 7E). Therefore, HeLa cells expressing Ly6a were infected significantly more by PHP.eB-A503 compared to control cells. Similarly, AAV-A503-Se2 transduced more HeLa cells that expressed Ly6c1 and to greater extent Ly6c2. AAV9-503 and AAV-A503-Se1 infection was not perturbed by the Ly6 GPI proteins exploited in this analysis.

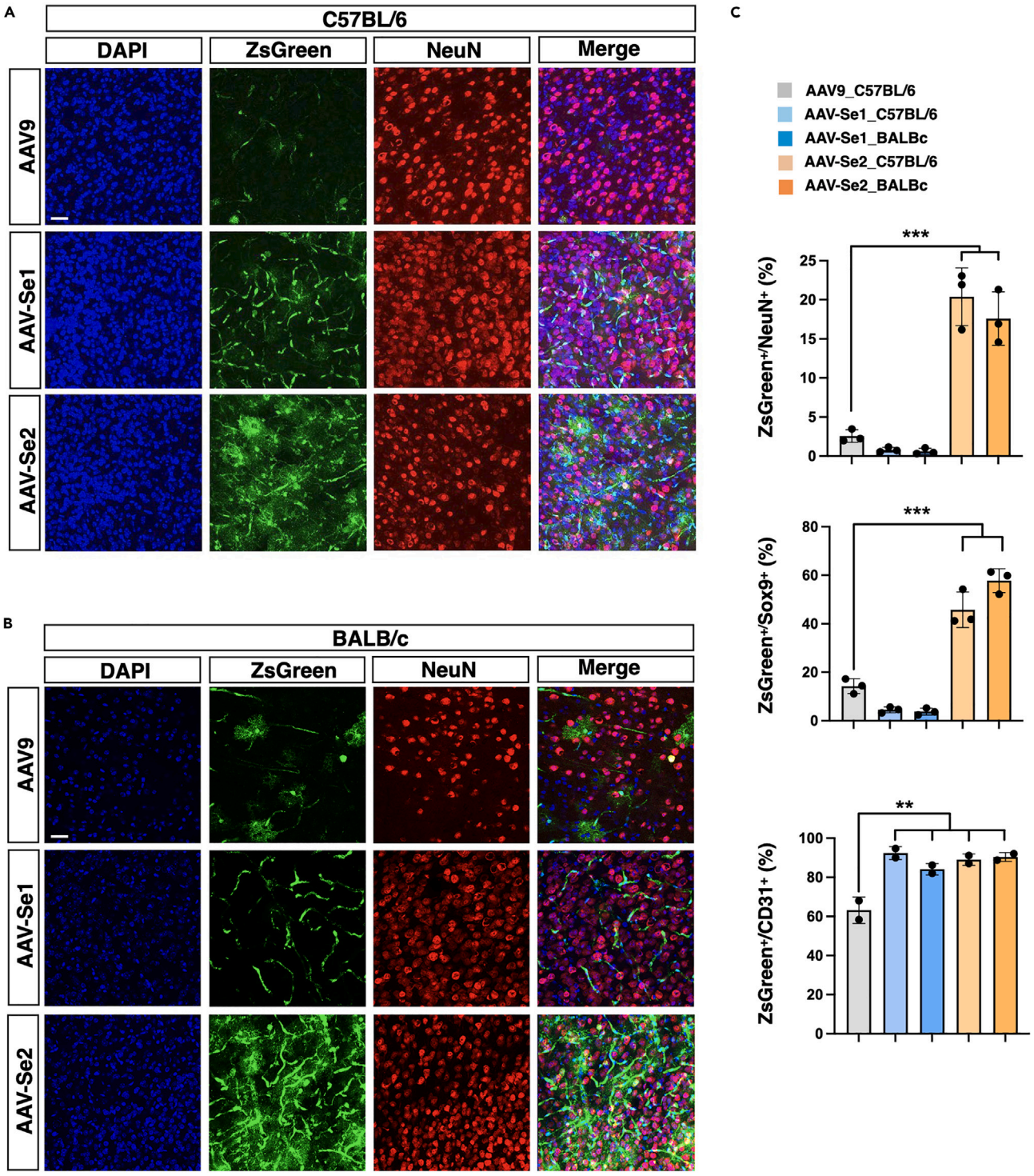

Figure 4. Cell-type specific analysis of the AAV-Se1/2 transduction pattern

(A and B) High magnification images of immunostainings for ZsGreen and NeuN (red) in cortices derived from C57BL/6 (A) and BALB/c (B) mice treated with AAV9, AAV-Se1 and AAV-Se2. Scale bars, 100 μm.

(C) Quantitative assessment of transduced (ZsGreen$^+$) neurons (NeuN$^+$), astrocytes (Sox9$^+$) and endothelial cells (CD31$^+$) in brain derived from AAV9, AAV-Se1 and AAV-Se2 treated C57BL/6 and BALB/c mice (n = 2–3 animals per group, 3 field per mice). Values are mean ± SD. ***$p < 0.001$. Statistical analysis is performed using one-way ANOVA followed by Tukey post-test.

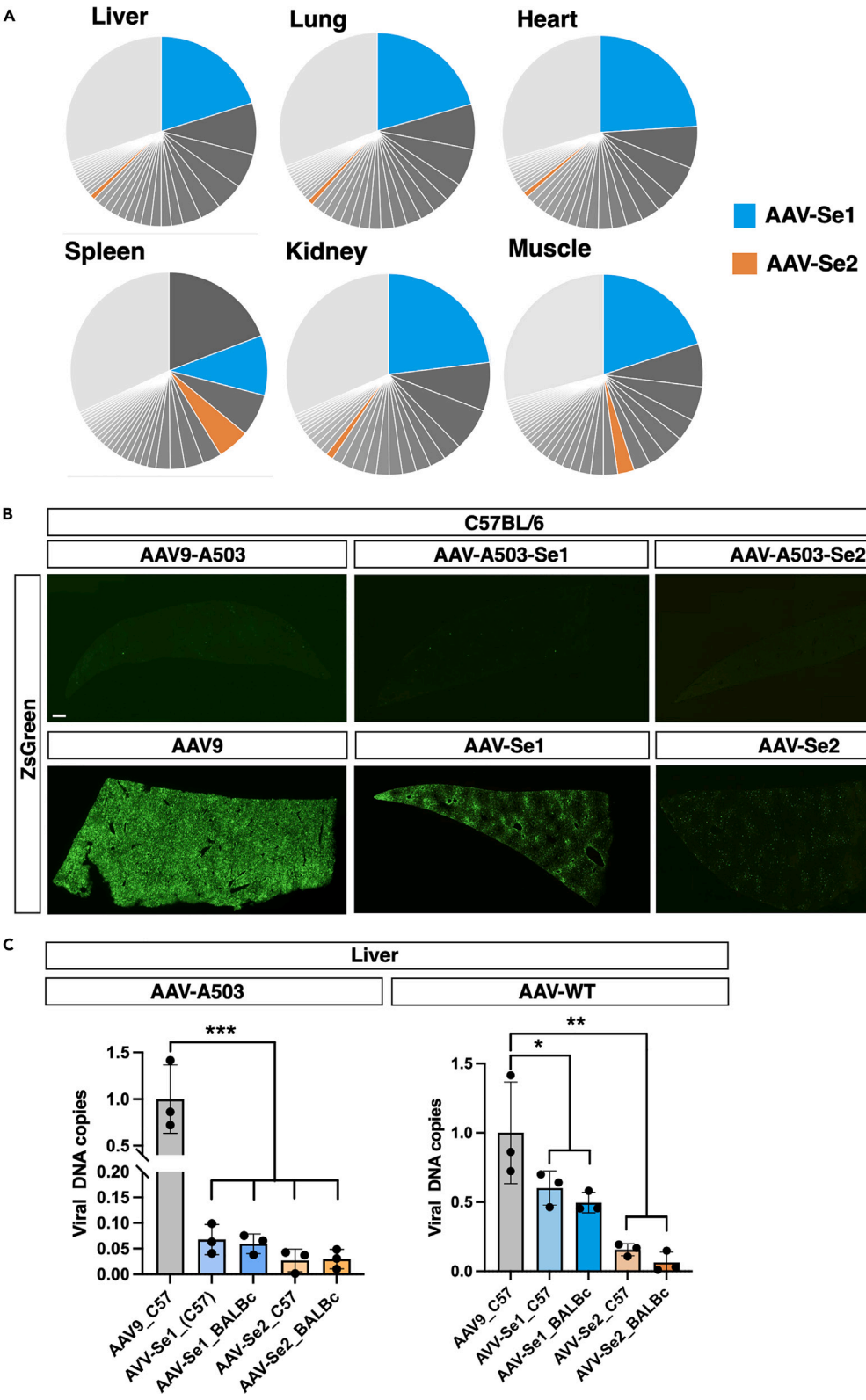
A
Liver
Lung
Heart
Spleen
Kidney
Muscle
AAV-Se1
AAV-Se2
B
C57BL/6
AAV9-A503
AAV-A503-Se1
AAV-A503-Se2
ZsGreen
AAV9
AAV-Se1
AAV-Se2
C
Liver
AAV-A503
AAV-WT
Viral DNA copies
***
**
*
AAV9_C57
AVV-Se1_(C57)
AAV-Se1_BALBc
AAV-Se2_C57
AAV-Se2_BALBc

Figure 5. AAV-Se1/2 exhibit a lower tropism for liver with respect to the parental AAV9

(A) Pie charts indicate the frequency of 7mer sequences determined by NGS in off-target organs, as in particular liver, lung, heart, spleen, kidney, and muscle, at the fourth and last round of selection. In all off-target organs AAV-Se2 (orange) sequence was less enriched then AAV-Se1 (blue).

(B) Low magnification immunostaining for ZsGreen in livers derived from C57BL/6 mice treated with AAV9, AAV-Se1 and AAV-Se2 with (bottom panels) or without (A503, upper panels) competence for galactose binding. Scale bars, 200 μm.

(C) Viral DNA vector quantification by qRT-PCR in livers from C57BL/6 and BALB/c mice treated with AAV9-A503, AAV-A503-Se1 and AAV-A503-Se2 (on the left) and AAV9, AAV-Se1 and AAV-Se2 (on the right). The results are reported as the fold change of viral ZsGreen DNA in mice treated with AAV-A503-Se1 and AAV-A503-Se2 (left) and AAV-Se1 and AAV-Se2 (right) relative to mice treated with AAV9 (n = 3 animals per group). Values are mean ± SD. *$p < 0.05$; **$p < 0.01$, ***$p < 0.001$. Statistical analysis is performed using one-way ANOVA followed by Tukey post-test.

AAV-BI30 with mutated galactose-binding domain significantly reduces liver targeting without affecting its brain transduction efficiency

Given that the loss of galactose binding on the AAV-Se1/2 dramatically reduced their off-targeting to the liver while mostly preserving their transduction efficiency for brain endothelial cells, we thought that the same approach could be extended to other endothelial-directed capsids. In particular, the AAV9 engineered capsid variant AAV-BI30 was recently showed to efficiently transduce the endothelial cells of the brain, retina and spinal cord vasculature after systemic delivery.[39] However, AAV-BI30 also exhibited an extensive tropism for peripheral organs, especially for liver, which could lead to hepatotoxicity in the treated mice.[39] Thus, in analogy to our previous results, we introduced the W503A mutation within the AAV-BI30 capsid to assess its impact of the infectivity profile of this capsid. As expected, the ZsGreen expressing AAV-A503-BI30 administrated intravenously at 1 x 10^{11} vg per mouse, sustained efficient gene transfer in the brain vasculature, but was associated with a greatly reduced tropism for the liver compared to the unmodified parental capsid (Figure 8). Thus, modulation of the galactose-binding ability of capsid variants may be an additional modification that has a major impact on limiting off-target viral infectivity in peripheral organs. In contrast, this change will not markedly affect the tropism of interest if this is mainly mediated by the engineered modification introduced into the capsid variant.

DISCUSSION

Herein, we described the isolation of two novel AAV9 engineered variants with a superior ability to target the brain after intravenous delivery by screening a new display peptide library developed from a galactose binding deficient AAV9 capsid. We speculated that this combination would erase the natural binding pattern of the mutant capsid, maximizing the selection of new capsid-cellular receptor interactions exquisitely dependent on the exogenous peptide. However, although the AAV-A503-Se1/2 viruses showed an efficient transduction of the brain vasculature, these capsids exhibit a very poor ability to infect brain cells. Only after restoration of the functional galactose binding site did both viruses acquired the ability to infect both neuronal and glial cells in the brain parenchyma. These results suggest that AAV9-like capsids may require two distinct domains to efficiently transduce the brain: the first necessary to bind and cross the endothelium which is provided by the exogenous peptide and the galactose binding to subsequently transduce the other brain cells. No case has yet been described where a single domain in the capsid can support both functions in the same virus. In this light, our approach was well suited to isolate peptides that could confer to the capsids an enhanced transduction of the endothelium, but without directly influencing the subsequent tropism toward either neuronal or glial cells, which is mainly controlled by the virus-galactose interaction.

While AAV-Se1 emerged already at the second cycle, the AAV-Se2 was found enriched only in the fourth and last selection round, suggesting that the dynamics of enrichment between the different capsid variants could be extremely different. This is reflected in the rather different peptide sequence selected in the two capsids and their probably different cell receptors. Both sequences are distinct from those of other previously selected variants, suggesting that the diversity offered by the randomized heptapeptide is extremely high, making it unlikely that the same exact sequences would be selected in independent experiments. The AAV-A503-Se1/2 viruses showed a very selective transduction of brain endothelial cells in both C57BL/6 and BALB/c mouse strains, with a minority of non-endothelial cells being infected. Furthermore, AAV-A503-Se1/2 exhibited an extremely low tropism for peripheral organs, including the liver, compared to the parental AAV9, thus avoiding the risk of systemic toxicity or off-target effects even when relatively high viral doses are administered intravenously. These viruses are therefore valuable tools for selective and efficient gene transfer within the brain vasculature with superior advantages over previous similar capsids. Conversely, after galactose binding reconstitution, the wild-type AAV-Se2, more than the AAV-Se1, acquired a high efficiency to transduce both neuronal and glial cells throughout the brain. In fact, AAV-Se2 transduction levels in the brain tissue were not significantly different from those sustained by the PHP.eB, one of the capsids with the highest brain targeting after intravenous delivery.[32] However, even in this case, the wild-type AAV-Se1/2 displayed a notably lower tropism for the liver compared to the unmodified AAV9, suggesting that the integrated peptides play a direct role in de-targeting AAV-Se1/2 capsids from this peripheral organ. We next evaluated the transduction rate of AAV-Se1/2 in the brain of adult marmosets. In a side-by-side comparison, we confirmed that these variants have a higher brain tropism compared to the unmodified AAV9. In particular, cerebellar Purkinje cells were efficiently transduced by the AAV-Se2, with an overall rate of more than 25%. This capsid therefore could represent an interesting tool for gene delivery for the treatment of genetic forms of ataxia caused by selective degeneration of this class of neurons. Of course, the limited number of marmosets used in this work is not sufficient to draw definitive conclusions. However, the two animals treated with the AAV-Se2 showed a comparable transduction profile, indicating a general reliability of the technical procedures applied uniformly to all the animals. Overall, the infectivity of both AAV-Se1/2 was generally lower in marmosets than in mice, suggesting a lack of conserved gene transfer efficiency in NHPs. For this reason, we considered evaluating

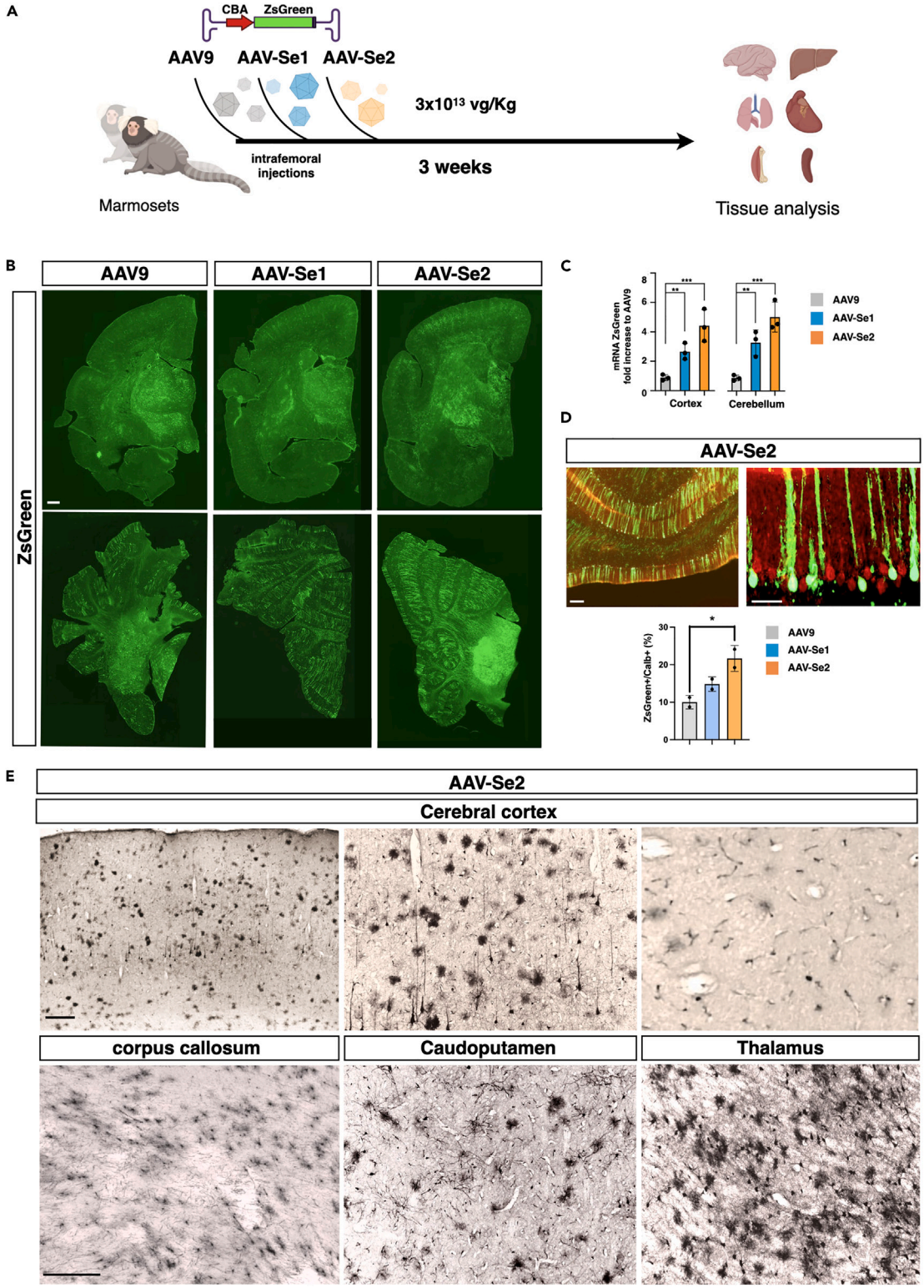

Figure 6. Brain transduction efficiency of AAV9 and AAV-Se1/2 in adult marmosets

(A) Illustration of the experimental setting. Adult marmosets were systemically injected with AAV9 (n = 1), AAV-Se1 (n = 1) and AAV-Se2 (n = 2) carrying the ZsGreen transgene under the control of the CBA strong constitutive promoter (experimental viral dose: 3 × 10^{13} vg/kg). After three weeks from the injections, marmosets were sacrificed for tissues analyses.

Figure 6. *Continued*

(B) Low magnification images of ZsGreen immunofluorescence in cerebrum (upper panel) and cerebellum (bottom panel) derived from marmoset treated with AAV9, AAV-Se1 and AAV-Se2. Scale bars, 200 μm.

(C) Bar graphs depicting fold change differences of ZsGreen mRNA levels in cortices and cerebella transduced with AAV-Se1/Se2 respect to AAV9 (n = 3 pieces for each tissue).

(D) Low (upper) and high (bottom) magnification images of immunostainings for ZsGreen and Calbindin (Calb) in the cerebellum derived from marmoset treated with AAV-Se2. Scale bars, 100 μm. Below, quantitative assessment of transduced ($ZsGreen^+$) Purkinje cells ($Calb^+$) in brain derived from AAV9, AAV-Se1 and AAV-Se2 treated marmosets (n = 3 different fields of each cerebellum).

(E) Representative images of immunohistochemistry for the reporter ZsGreen expressed by the AAV-Se2 in in selected brain regions such as cerebral cortex, corpus callosum, caudoputamen, and thalamus. Values are mean ± SD. *$p < 0.05$; **$p < 0.01$, ***$p < 0.001$. Statistical analysis is performed using one-way ANOVA followed by Tukey post-test.

the dependence of these viruses on receptors already implicated in the virus-cell interactions. First, we set up an *in vitro* assay to determine the efficiency of viral transduction on HeLa cells expressing a candidate viral receptor. To validate the system, we showed that only cells expressing the receptor Ly6a are robustly transduced by the PHP.eB virus. Ly6A belongs to a large superfamily of small proteins with an LU domain composed of 80 amino acids containing ten cysteines, forming a three-fingers spatial configuration.[40,41] Although the mouse genome contains 61 Ly6 members, Ly6A shares the highest homology with proteins encoded by neighboring genes within the same genomic locus, forming the so-called Ly6A sub-family, which has been largely deleted during mammalian evolution.[42] Surveying the expression profile from publicly available databases, we found that among these homologues, Ly6C1 has the highest and most selective expression in brain endothelial cells, similar to Ly6A. Remarkably, we found that transduction of AAV-Se2 was greatly enhanced in cells expressing either Ly6c1 or its close homologue Ly6c2, suggesting that these are plausible receptors for this capsid. We also found that AAV-Se2 infectivity can be augmented in cells expressing Ly6e. Thus, the enhanced brain transduction of AAV-Se2 compared to AAV9 in NHPs is likely mediated by Ly6E which, contrary to Ly6c1/2, is conserved throughout mammalian evolution. Moreover, given that endothelial expression of Ly6c1 and Ly6e is largely confined to the brain, this would contextualize the very poor tropism of AAV-Se2 that we observed in the peripheral organs in both mice and NHPs. In contrast, we noted that the basal levels of transduction in cells not expressing any murine Ly6 GPI proteins were significantly higher for AAV-Se1. Thus, this capsid has acquired other properties that have positively influenced its infectivity, which may explain its high and selective transduction of the brain endothelium.

Our study clearly demonstrated that viral tropism can be modulated in a combinatorial manner by modifying the galactose-binding domain in AAV9 engineered capsids. This option has remained poorly exploited in the field, while we have shown that it can be used to minimize or prevent the tropism to liver and other peripheral organs, while preserving infectivity to the tissue targeted through the displayed peptide. We provide evidence that this approach can be generalized to other viral vectors by showing that the strong liver tropism of the AAV-BI30 capsid can be significantly attenuated, although not to the minimal levels of the AAV-A503-Se1/2 variants, while maintaining its infectivity of the brain endothelium unaltered. We postulate that the same modification could work with several other engineered capsids to enhance their safety profile. Thus, this option further expands the possible targeted manipulations on the capsid variants to control their viral transduction pattern and significantly minimize off-target tropism, which are indispensable features to nominate them for clinical use.

Limitations of the study

The brain tropism of AAV-Se1/2 capsids in marmosets was inferred from a limited number of animals, and therefore definitive conclusions on the extent of improved infectivity compared to the parental AAV9 await more comprehensive analysis with additional animals. Moreover, marmosets are New World monkeys that diverged from ape evolution about 30 million years ago and, thus, AAV-Se1/2 capsid brain tropism should be confirmed in Old World monkeys, such as Macaca, to gain further evidence of clinical relevance. Our results revealed a selective and high tropism of the AAV-Se1 capsid for the brain endothelium. However, recent studies have reported the isolation of other AAV engineered capsids with a pronounced brain endothelial targeting.[39,43] Therefore, a side-by-side comparison between these capsids and AAV-Se1 is warranted to determine the variant with the highest ratio of brain endothelium to off-target infectivity.

STAR★METHODS

Detailed methods are provided in the online version of this paper and include the following:

- KEY RESOURCES TABLE
- RESOURCE AVAILABILITY
  - Lead contact
  - Materials availability
  - Data and code availability
- METHOD DETAILS
  - Cell lines
  - Primary cell cultures
  - Mice
  - Marmosets

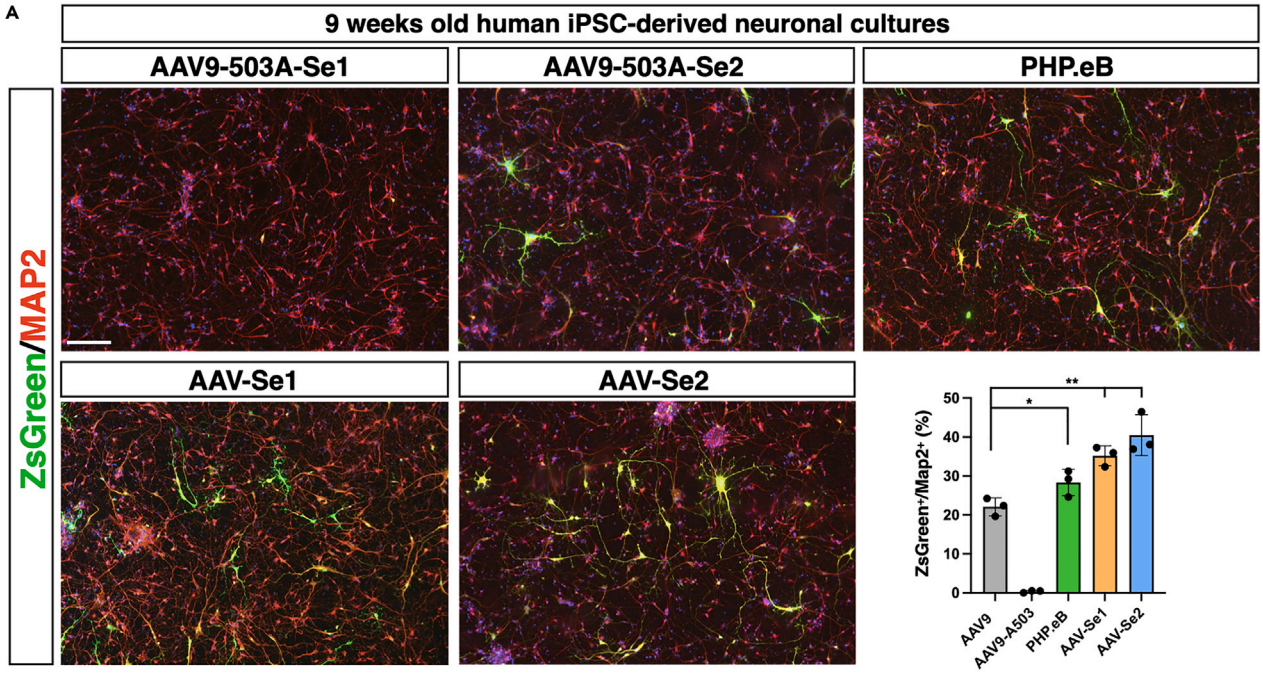
A
9 weeks old human iPSC-derived neuronal cultures
AAV9-503A-Se1
AAV9-503A-Se2
PHP.eB
AAV-Se1
AAV-Se2
ZsGreen/MAP2
ZsGreen+/Map2+ (%)
AAV9
AAV9-A503
PHP.eB
AAV-Se1
AAV-Se2

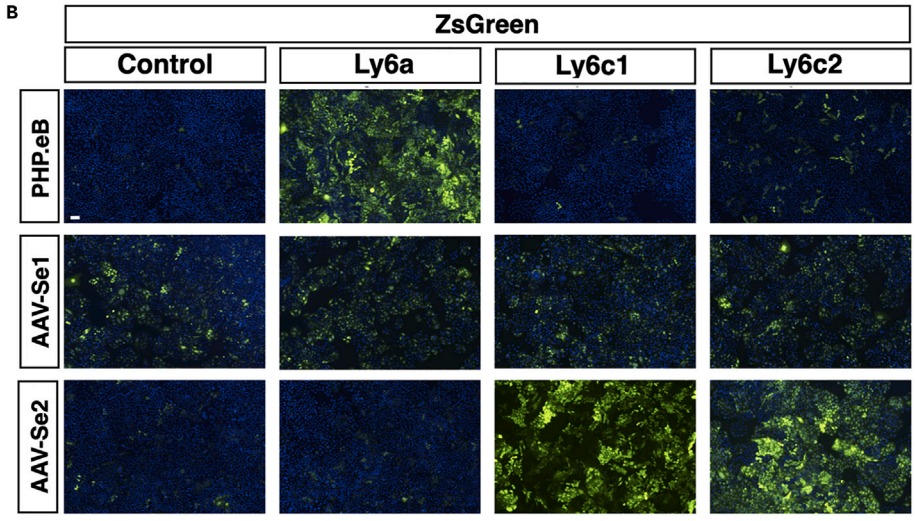
B
ZsGreen
Control
Ly6a
Ly6c1
Ly6c2
PHP.eB
AAV-Se1
AAV-Se2

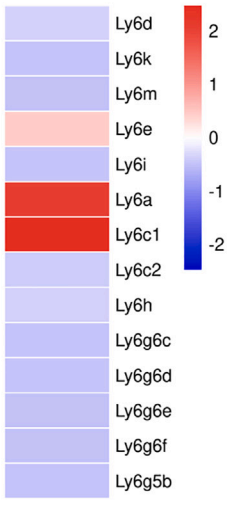
C
Ly6d
Ly6k
Ly6m
Ly6e
Ly6i
Ly6a
Ly6c1
Ly6c2
Ly6h
Ly6g6c
Ly6g6d
Ly6g6e
Ly6g6f
Ly6g5b

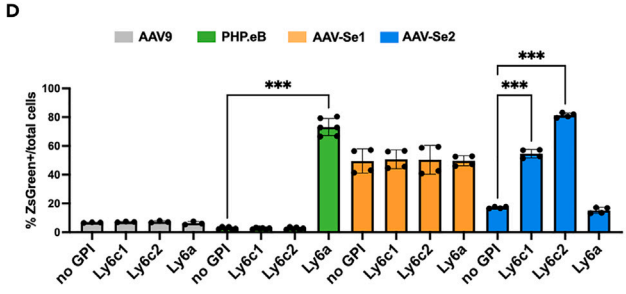
D
AAV9
PHP.eB
AAV-Se1
AAV-Se2
% ZsGreen+/total cells
no GPI
Ly6c1
Ly6c2
Ly6a

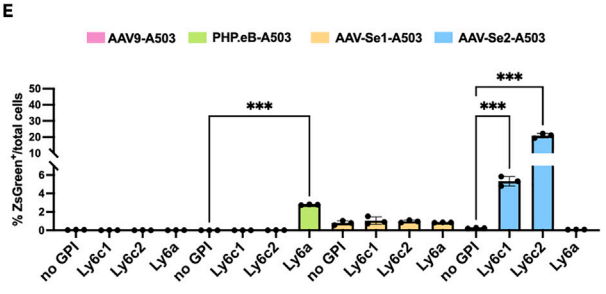
E
AAV9-A503
PHP.eB-A503
AAV-Se1-A503
AAV-Se2-A503
% ZsGreen+/total cells
no GPI
Ly6c1
Ly6c2
Ly6a

Figure 7. Viral transduction efficiency in human neurons and testing of Ly6 proteins as candidate receptors for AAV-Se1/2 capsids

(A) Immunostaining for ZsGreen and MAP2 in hiPSCs-derived neurons transduced with AAV9-A503, AAV9, PHP.eB, AAV-Se1 or AAV-Se2 viral vectors. Bottom right, quantification of ZsGreen$^+$ on total number of MAP2$^+$ (n = 3 independent experiments). Scale bar, 100 μm.

(B) ZsGreen immunofluorescence in HeLa cells transfected with Ly6a, Ly6c1, Ly6c2 or untransfected (control) and subsequently transduced with ZsGreen expressing PHP.eB, AAV-Se1 or AAV-Se2 viral vectors. Scale bars, 100 μm.

(C) Relative expression levels of Ly6 genes in brain endothelial cells as elaborated from a publicly available scRNA-seq dataset (https://doi.org/10.22002/D1.2090).

(D and E) Quantification by flow cytometry of ZsGreen positive HeLa cells transfected with Ly6a, Ly6c1, Ly6c2 or untransfected (control) and subsequently transduced with ZsGreen expressing AAV9, PHP.eB, AAV-Se1 or AAV-Se2 viral vectors (D) or AAV9-A503, PHP.eB-503, AAV-Se1-A503 and AAV-Se2-A503 viral vectors (E). Values are mean ± SD of n = 3 independent experiments. *p < 0.05; **p < 0.01, ***p < 0.001. Statistical analysis is performed using one-way ANOVA followed by Tukey post-test.

- *In vivo* screening of the random AAV9 display peptide library
- Next-generation sequencing
- Computational analysis
- Generation of packaging plasmids and gene transfer vectors
- AAV virus production and purification
- Lentivirus virus production and purification
- *In vivo* administration of AAV vectors in mice and tissue collection
- Testing basal immunity to AAV capsids in NHPs
- *In vivo* administration of AAV vectors in marmosets and tissue collection
- Immunofluorescence
- Acquisition and quantification of immunofluorescent images
- Determination of vector copy numbers by qPCR

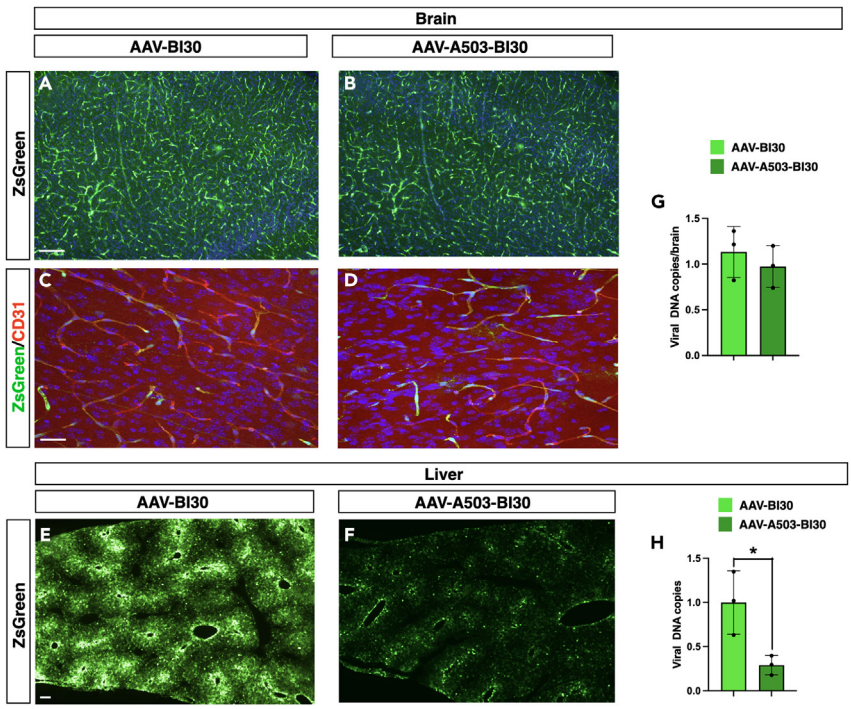

Figure 8. Effective liver de-targeting by inserting the A503 mutation in the AAV-BI30 capsid

(A–D) Single ZsGreen (A,B) or double ZsGreen/CD31 (C,D) immunofluorescence staining highlighting the enriched endothelial the transduction of the unmodified AAV-BI30 (A,C) and its mutant form AAV-BI30-A503 (B,D) capsid. Scale bars, 100 μm.

(E and F) Representative images of ZsGreen immunofluorescence levels in liver of mice intravenously injected with the unmodified AAV-BI30 (E) and its mutant form AAV-BI30-A503 (F) capsid. Scale bar, 200 μm.

(G and H) Viral DNA copies quantification by qPCR in brain (G) and liver (H) tissues transduced with either unmodified AAV-BI30 or its mutant form AAV-BI30-A503 capsid. Values are mean ± SD of n = 3 independent experiments. *p < 0.05. Statistical analysis is performed using unpaired t test.

- CRISPR/Cas9 gene editing in HeLa cells
- Transduction assay in neuronal and cell cultures

- QUANTIFICATION AND STATISTICAL ANALYSIS

SUPPLEMENTAL INFORMATION

Supplemental information can be found online at https://doi.org/10.1016/j.isci.2024.109777.

ACKNOWLEDGMENTS

We thank L. Naldini for providing valuable reagents as well as T. Sieber and M. Trepel for generating and providing the p9K7 plasmid library. We are grateful to all members of the Broccoli's lab for helpful discussions. We acknowledge the FRACTAL and ALEMBIC core facilities for expert supervision in flow-cytometry and confocal imaging, respectively. This work was supported by the grant CN00000041 "National Center for Gene Therapy and Drugs based on RNA Technology" (concession number 1035 of 17 June 2022-PNRR MUR - M4C2 - Investment 1.4 Call "National Centers", financed by EU- NextGenerationEU).

AUTHOR CONTRIBUTIONS

S.S.G. and M.L. performed all the experiments and analyzed data; A.I. analyzed viral infections in iPSC-derived neuronal cultures; I.P. supervised the work with marmosets; J.M. oversighted the license and ethical permissions for experimental procedures in primates; J.K. supervised the plasmid and viral library generation; S.B. contributed to immunohistochemistry and image analysis; V.B. supervised, coordinated and supported the project and wrote the manuscript.

DECLARATION OF INTERESTS

The authors have filed a patent application for the work described in this manuscript.

Received: November 10, 2023
Revised: February 28, 2024
Accepted: April 15, 2024
Published: April 18, 2024

REFERENCES

1. Kuzmin, D.A., Shutova, M.V., Johnston, N.R., Smith, O.P., Fedorin, V.V., Kukushkin, Y.S., van der Loo, J.C.M., and Johnstone, E.C. (2021). The clinical landscape for AAV gene therapies. Nat. Rev. Drug Discov. *20*, 173–174.
2. Hudry, E., and Vandenberghe, L.H. (2019). Therapeutic AAV Gene Transfer to the Nervous System: A Clinical Reality. Neuron *101*, 839–862.
3. Deverman, B.E., Ravina, B.M., Bankiewicz, K.S., Paul, S.M., and Sah, D.W.Y. (2018). Gene therapy for neurological disorders: progress and prospects. Nat. Rev. Drug Discov. *17*, 641–659.
4. Bedbrook, C.N., Deverman, B.E., and Gradinaru, V. (2018). Viral Strategies for Targeting the Central and Peripheral Nervous Systems. Annu. Rev. Neurosci. *41*, 323–348.
5. Hocquemiller, M., Giersch, L., Audrain, M., Parker, S., and Cartier, N. (2016). Adeno-Associated Virus-Based Gene Therapy for CNS Diseases. Hum. Gene Ther. *27*, 478–496.
6. Gessler, D.J., and Gao, G. (2016). Gene Therapy for the Treatment of Neurological Disorders: Metabolic Disorders. Methods Mol. Biol. *1382*, 429–465.
7. Wang, D., Tai, P.W.L., and Gao, G. (2019). Adeno-associated virus vector as a platform for gene therapy delivery. Nat. Rev. Drug Discov. *18*, 358–378.
8. Grimm, D., and Büning, H. (2017). Small But Increasingly Mighty: Latest Advances in AAV Vector Research, Design, and Evolution. Hum. Gene Ther. *28*, 1075–1086.
9. Jan, A., Richner, M., Vægter, C.B., Nyengaard, J.R., and Jensen, P.H. (2019). Gene Transfer in Rodent Nervous Tissue Following Hindlimb Intramuscular Delivery of Recombinant Adeno-Associated Virus Serotypes AAV2/6, AAV2/8, and AAV2/9. Neurosci. Insights *14*, 1179069519889022.
10. Colella, P., Ronzitti, G., and Mingozzi, F. (2018). Emerging Issues in AAV-Mediated *In Vivo* Gene Therapy. Mol. Ther. Methods Clin. Dev. *8*, 87–104.
11. Zincarelli, C., Soltys, S., Rengo, G., and Rabinowitz, J.E. (2008). Analysis of AAV serotypes 1-9 mediated gene expression and tropism in mice after systemic injection. Mol. Ther. *16*, 1073–1080.
12. Gao, G., Lu, Y., Calcedo, R., Grant, R.L., Bell, P., Wang, L., Figueredo, J., Lock, M., and Wilson, J.M. (2006). Biology of AAV serotype vectors in liver-directed gene transfer to nonhuman primates. Mol. Ther. *13*, 77–87.
13. Pupo, A., Fernández, A., Low, S.H., François, A., Suárez-Amarán, L., and Samulski, R.J. (2022). AAV vectors: The Rubik's cube of human gene therapy. Mol. Ther. *30*, 3515–3541.
14. Li, C., and Samulski, R.J. (2020). Engineering adeno-associated virus vectors for gene therapy. Nat. Rev. Genet. *21*, 255–272.
15. El Andari, J., and Grimm, D. (2021). Production, Processing, and Characterization of Synthetic AAV Gene Therapy Vectors. Biotechnol. J. *16*, e2000025.
16. Lee, E.J., Guenther, C.M., and Suh, J. (2018). Adeno-Associated Virus (AAV) Vectors: Rational Design Strategies for Capsid Engineering. Curr. Opin. Biomed. Eng. *7*, 58–63.
17. Vandenberghe, L.H., Wilson, J.M., and Gao, G. (2009). Tailoring the AAV vector capsid for gene therapy. Gene Ther. *16*, 311–319.
18. Müller, O.J., Kaul, F., Weitzman, M.D., Pasqualini, R., Arap, W., Kleinschmidt, J.A., and Trepel, M. (2003). Random peptide libraries displayed on adeno-associated virus to select for targeted gene therapy vectors. Nat. Biotechnol. *21*, 1040–1046.
19. Perabo, L., Büning, H., Kofler, D.M., Ried, M.U., Girod, A., Wendtner, C.M., Enssle, J., and Hallek, M. (2003). In vitro selection of viral vectors with modified tropism: the adeno-associated virus display. Mol. Ther. *8*, 151–157.
20. Summerford, C., and Samulski, R.J. (1998). Membrane-associated heparan sulfate proteoglycan is a receptor for adeno-associated virus type 2 virions. J. Virol. *72*, 1438–1445.
21. Körbelin, J., Sieber, T., Michelfelder, S., Lunding, L., Spies, E., Hunger, A., Alawi, M., Rapti, K., Indenbirken, D., Müller, O.J., et al. (2016). Pulmonary Targeting of Adeno-associated Viral Vectors by Next-generation Sequencing-guided Screening of Random Capsid Displayed Peptide Libraries. Mol. Ther. *24*, 1050–1061.
22. Körbelin, J., Dogbevia, G., Michelfelder, S., Ridder, D.A., Hunger, A., Wenzel, J., Seismann, H., Lampe, M., Bannach, J., Pasparakis, M., et al. (2016). A brain microvasculature endothelial cell-specific viral vector with the potential to treat

neurovascular and neurological diseases. EMBO Mol. Med. *8*, 609–625.
23. Michelfelder, S., Kohlschütter, J., Skorupa, A., Pfennings, S., Müller, O., Kleinschmidt, J.A., and Trepel, M. (2009). Successful expansion but not complete restriction of tropism of adeno-associated virus by in vivo biopanning of random virus display peptide libraries. PLoS One *4*, e5122.
24. Meumann, N., Cabanes-Creus, M., Ertelt, M., Navarro, R.G., Lucifora, J., Yuan, Q., Nien-Huber, K., Abdelrahman, A., Vu, X.K., Zhang, L., et al. (2023). Adeno-associated virus serotype 2 capsid variants for improved liver-directed gene therapy. Hepatology *77*, 802–815.
25. Rode, L., Bär, C., Groß, S., Rossi, A., Meumann, N., Viereck, J., Abbas, N., Xiao, K., Riedel, I., Gietz, A., et al. (2022). AAV capsid engineering identified two novel variants with improved in vivo tropism for cardiomyocytes. Mol. Ther. *30*, 3601–3618.
26. Michelfelder, S., Varadi, K., Raupp, C., Hunger, A., Körbelin, J., Pahrmann, C., Schrepfer, S., Müller, O.J., Kleinschmidt, J.A., and Trepel, M. (2011). Peptide ligands incorporated into the threefold spike capsid domain to re-direct gene transduction of AAV8 and AAV9 in vivo. PLoS One *6*, e23101.
27. Varadi, K., Michelfelder, S., Korff, T., Hecker, M., Trepel, M., Katus, H.A., Kleinschmidt, J.A., and Müller, O.J. (2012). Novel random peptide libraries displayed on AAV serotype 9 for selection of endothelial cell-directed gene transfer vectors. Gene Ther. *19*, 800–809.
28. Shen, S., Bryant, K.D., Brown, S.M., Randell, S.H., and Asokan, A. (2011). Terminal N-linked galactose is the primary receptor for adeno-associated virus 9. J. Biol. Chem. *286*, 13532–13540.
29. Bell, C.L., Vandenberghe, L.H., Bell, P., Limberis, M.P., Gao, G.P., Van Vliet, K., Agbandje McKenna, M., and Wilson, J.M. (2011). The AAV9 receptor and its modification to improve in vivo lung gene transfer in mice. J. Clin. Invest. *121*, 2427–2435.
30. Bell, C.L., Gurda, B.L., Van Vliet, K., Agbandje-McKenna, M., and Wilson, J.M. (2012). Identification of the galactose binding domain of the adeno-associated virus serotype 9 capsid. J. Virol. *86*, 7326–7333.
31. Deverman, B.E., Pravdo, P.L., Simpson, B.P., Kumar, S.R., Chan, K.Y., Banerjee, A., Wu, W.L., Yang, B., Huber, N., Pasca, S.P., and Gradinaru, V. (2016). Cre-dependent selection yields AAV variants for widespread gene transfer to the adult brain. Nat. Biotechnol. *34*, 204–209.
32. Chan, K.Y., Jang, M.J., Yoo, B.B., Greenbaum, A., Ravi, N., Wu, W.L., Sánchez-Guardado, L., Lois, C., Mazmanian, S.K., Deverman, B.E., and Gradinaru, V. (2017). Engineered AAVs for efficient noninvasive gene delivery to the central and peripheral nervous systems. Nat. Neurosci. *20*, 1172–1179.
33. Hordeaux, J., Wang, Q., Katz, N., Buza, E.L., Bell, P., and Wilson, J.M. (2018). The Neurotropic Properties of AAV-PHP.B Are Limited to C57BL/6J Mice. Mol. Ther. *26*, 664–668.
34. Hordeaux, J., Yuan, Y., Clark, P.M., Wang, Q., Martino, R.A., Sims, J.J., Bell, P., Raymond, A., Stanford, W.L., and Wilson, J.M. (2019). The GPI-Linked Protein LY6A Drives AAV-PHP.B Transport across the Blood-Brain Barrier. Mol. Ther. *27*, 912–921.
35. Huang, Q., Chan, K.Y., Tobey, I.G., Chan, Y.A., Poterba, T., Boutros, C.L., Balazs, A.B., Daneman, R., Bloom, J.M., Seed, C., and Deverman, B.E. (2019). Delivering genes across the blood-brain barrier: LY6A, a novel cellular receptor for AAV-PHP.B capsids. PLoS One *14*, e0225206.
36. Batista, A.R., King, O.D., Reardon, C.P., Davis, C., Shankaracharya, P.,V., Philip, V., Gray-Edwards, H., Aronin, N., Lutz, C., Landers, J., and Sena-Esteves, M. (2020). *Ly6a* Differential Expression in Blood-Brain Barrier Is Responsible for Strain Specific Central Nervous System Transduction Profile of AAV-PHP.B. Hum. Gene Ther. *31*, 90–102.
37. Weinmann, J., Weis, S., Sippel, J., Tulalamba, W., Remes, A., El Andari, J., Herrmann, A.K., Pham, Q.H., Borowski, C., Hille, S., et al. (2020). Identification of a myotropic AAV by massively parallel in vivo evaluation of barcoded capsid variants. Nat. Commun. *11*, 5432.
38. Tabebordbar, M., Lagerborg, K.A., Stanton, A., King, E.M., Ye, S., Tellez, L., Krunnfusz, A., Tavakoli, S., Widrick, J.J., Messemer, K.A., et al. (2021). Directed evolution of a family of AAV capsid variants enabling potent muscle-directed gene delivery across species. Cell *184*, 4919–4938.e22.
39. Krolak, T., Chan, K.Y., Kaplan, L., Huang, Q., Wu, J., Zheng, Q., Kozareva, V., Beddow, T., Tobey, I.G., Pacouret, S., et al. (2022). A High-Efficiency AAV for Endothelial Cell Transduction Throughout the Central Nervous System. Nat. Cardiovasc. Res. *1*, 389–400.
40. Loughner, C.L., Bruford, E.A., McAndrews, M.S., Delp, E.E., Swamynathan, S., and Swamynathan, S.K. (2016). Organization, evolution and functions of the human and mouse Ly6/uPAR family genes. Hum. Genom. *10*, 10.
41. Vasilyeva, N.A., Loktyushov, E.V., Bychkov, M.L., Shenkarev, Z.O., and Lyukmanova, E.N. (2017). Three-Finger Proteins from the Ly6/uPAR Family: Functional Diversity within One Structural Motif. Biochemistry *82*, 1702–1715.
42. Shmerling, M., Chalik, M., Smorodinsky, N.I., Meeker, A., Roy, S., Sagi-Assif, O., Meshel, T., Danilevsky, A., Shomron, N., Levinger, S., et al. (2022). LY6S, a new IFN-inducible human member of the Ly6a subfamily expressed by spleen cells and associated with inflammation and viral resistance. Immunohorizons *6*, 253–272.
43. Chen, X., Wolfe, D.A., Bindu, D.S., Zhang, M., Taskin, N., Goertsen, D., Shay, T.F., Sullivan, E.E., Huang, S.F., Ravindra Kumar, S., et al. (2023). Functional gene delivery to and across brain vasculature of systemic AAVs with endothelial-specific tropism in rodents and broad tropism in primates. Nat. Commun. *14*, 3345.
44. Iannielli, A., Luoni, M., Giannelli, S.G., Ferese, R., Ordazzo, G., Fossati, M., Raimondi, A., Opazo, F., Corti, O., Prehn, J.H.M., et al. (2022). Modeling native and seeded Synuclein aggregation and related cellular dysfunctions in dopaminergic neurons derived by a new set of isogenic iPSC lines with SNCA multiplications. Cell Death Dis. *13*, 881.
45. Körbelin, J., and Trepel, M. (2017). How to Successfully Screen Random Adeno-Associated Virus Display Peptide Libraries In Vivo. Hum Gene Ther. Methods *28*, 109–123.
46. Luoni, M., Giannelli, S., Indrigo, M.T., Niro, A., Massimino, L., Iannielli, A., Passeri, L., Russo, F., Morabito, G., Calamita, P., et al. (2020). Whole brain delivery of an instability-prone Mecp2 transgene improves behavioral and molecular pathological defects in mouse models of Rett syndrome. Elife *9*, e52629.
47. Schneider, C.A., Rasband, W.S., and Eliceiri, K.W. (2012). NIH Image to ImageJ: 25 years of image analysis. Nat. Methods *9*, 671–675.
48. Concordet, J.P., and Haeussler, M. (2018). CRISPOR: intuitive guide selection for CRISPR/Cas9 genome editing experiments and screens. Nucleic Acids Res. *46*, W242–W245.
49. Brinkman, E.K., Chen, T., Amendola, M., and van Steensel, B. (2014). Easy quantitative assessment of genome editing by sequence trace decomposition. Nucleic Acids Res. *42*, e168.
50. Rubio, A., Luoni, M., Giannelli, S.G., Radice, I., Iannielli, A., Cancellieri, C., Di Berardino, C., Regalia, G., Lazzari, G., Menegon, A., et al. (2016). Rapid and efficient CRISPR/Cas9 gene inactivation in human neurons during human pluripotent stem cell differentiation and direct reprogramming. Sci. Rep. *6*, 37540.

STAR★METHODS

KEY RESOURCES TABLE

REAGENT or RESOURCE	SOURCE	IDENTIFIER
Antibodies		
Living Colors® Full-Length ZsGreen Polyclonal Antibody	Takara Bio	Cat#632474; RRID: AB_2491179
Living Colors® ZsGreen Monoclonal Antibody	Takara Bio	Cat#632598; RRID: AB_4398325
Rabbit polyclonal anti-NeuN	Abcam	Cat#ab104225; RRID: AB_10711153
Rabbit polyclonal anti-Calbindin	Swant	Cat# CB38; RRID: AB_10000340
Rat polyclonal anti-mouse CD31	BD Biosciences	Cat# 550274; RRID: AB_393571
Chicken polyclonal anti-MAP2	Abcam	Cat# ab92434; RRID: AB_2138147
Rabbit polyclonal anti-Olig2	MERCK	Cat# AB9610; RRID: AB_570666
Chicken monoclonal anti-Iba1	SYSY	Cat# 234009; RRID: AB_2891282
Rabbit polyclonal anti-Sox9	MERCK	Cat# ab5535; RRID: AB_2239761
Bacterial and virus strains		
AAV9-CBA-ZsGreen	This paper	N/A
AAV9-CBA-Luciferase2	This paper	N/A
AAV_PHP.eB-CBA-ZsGreen	This paper	N/A
AAV_503_PHP.eB-CBA-ZsGreen	This paper	N/A
AAV9_W503-CBA-ZsGreen	This paper	N/A
AAV_W503A_Se1-CBA-ZsGreen	This paper	N/A
AAV_W503A_Se2-CBA-ZsGreen	This paper	N/A
AAV_Se1-CBA-ZsGreen	This paper	N/A
AAV_Se2-CBA-ZsGreen	This paper	N/A
LV-Ef1a-mLy6a	This paper	N/A
LV-Ef1a-mLy6c1	This paper	N/A
LV-Ef1a-mLy6c2	This paper	N/A
ElectroMAX™ DH5alpha competent cells	ThemoFisher Scientific	Cat# 11319019
Chemicals, peptides, and recombinant proteins		
Sequenase enzyme	ThermoFisher Scientific	Cat# 70775Y200UN
SfiI enzyme	NEB	Cat# R0123L
BglI enzyme	NEB	Cat# R0143L
SapI enzyme	NEB	Cat# R0569L
AfeI enzyme	NEB	Cat# R0652L
NheI-HF enzyme	NEB	Cat# R3131L
AgeI-HF enzyme	NEB	Cat# R3552L
Luria Broth (LB)	MERCK	Cat# L3022-1kg
Ampicillin	MERCK	Cat# A9518
PolyFect Transfection Reagent	Qiagen	Cat# 301105
polyethyleneglicol 8000	MERCK	Cat# P2139
OptiPrep™ (Iodixanol commercial solution)	MERCK	Cat# D1556
Polyethylenimine 25K (PEI-25K)	Polyscience	Cat# 23966-1
Salt Active Nuclease (SAN)	ArticZyme	Cat# 70900-202
Amicon Ultra15 100kDa	MERCK	Cat# UFC10096
Paraformaldehyde	MERCK	Cat# 441244

(*Continued on next page*)

Continued

REAGENT or RESOURCE	SOURCE	IDENTIFIER
Sucrose	MERCK	Cat# S7903
Pooled Human Sera (PHS)	Dunn Labortechnik GmbH	Cat# ISERLY1GM
Triton X-100	MERCK	Cat# X100
PBS	MERCK	Cat# P4417
Fluorescence Mounting Medium	Agilent	Cat# S3023
VECTASTAIN ABC-HRP Kit	Vector Laboratories	Cat# PK-6100
OCT Embedding matrix for frozen sections	VWR	Cat# 361603E
Trypsin-EDTA (0.05%), phenol red	ThermoFisher	Cat# 25300062
Dulbecco's Modified Eagle Meadium (DMEM)	MERCK	Cat# D5671
Fetal Bovine Serum (FBS)	MERCK	Cat# F7524
Pennicillin/Streptomycin solution 100X	MERCK	Cat# P0781
Glutamine solution 200mM	MERCK	Cat# G7513
Sodium Pyruvate solution 100X	MERCK	Cat# S8636
MEM Non-Essential Amino acid 100X	MERCK	Cat# M7145
Puromycin	MERCK	Cat# P8833
Lipofectamine LTX reagent with PLUS reagent	ThermoFisher Scientific	Cat# 15338100
T7 endonuclease	NEB	CAT# M0302L
Blasticidin	ThermoFisher Scientific	Cat# R210-01
DNasi I ricombinant	MERCK	Cat# 04716728001
Hank's buffered salt solution (HBSS) no Ca^{2+} no Mg^{+}	Euroclone	Cat# ECB4007L
Neurobasal™ Medium	ThermoFisher Scientific	Cat# 21103049
poly-L-lysine	MERCK	Cat# P2636
B27 supplement (50X) serum free	ThermoFisher Scientific	Cat# 17504-001
SU5402	MERCK	Cat# SML0443
PD0325901	MERCK	Cat# PZ0162
DAPT	MERCK	Cat# D5942
Accutase	MERCK	Cat# A6964
Laminin	MERCK	Cat# L2020
Fibronectin	MERCK	Cat# F0895
Y27632	Selleckchem	Cat# S1049
BDNF	PeproTech	Cat# 450-02
Ascorbic Acid	MERCK	Cat# A4034
Dibutyryl cAMP	MERCK	Cat# D0627
Critical commercial assays		
NucleoBond Xtra MIDI plasmid	Macherey-Nagel	Cat# 740410.100
QIAquick Nucleotide Removal Kit	Qiagen	Cat# 28104
DNeasy Tissue Kit	Qiagen	Cat# 69504
AAVpro Titration Kit Ver2	Takara Bio	Cat# 6233
Bright-Glo™ Luciferase Assay System	Promega	Cat# E2620
Qiagen DNeasy Blood & Tissue Kits	Qiagen	Cat# 69506
Experimental models: Cell lines		
Human: 293T HEK cells	ATCC	CRL-3216
Human: HeLa	ATCC	CCL-2
Human: induced-Pluripotente Stem Cells (iPS)	Broccoli Vania	Iannielli et al.[44]

(*Continued on next page*)

Continued

REAGENT or RESOURCE	SOURCE	IDENTIFIER
Experimental models: Organisms/strains		
Mouse: C57BL/6	Charles River	027C57BL/6
Mouse: BALBc	Charles River	028BALB/C
Callithrix jacchus	Biomedical Primate Research Center (BPRC)	N/A
Oligonucleotides		
degenerate oligonucleotide encoding seven random amino acids (NNK): AGAGTGGCCAAGCAGGC(NNK)$_{7}$GCCCAGGCGGCCACCGGC	Metabion	N/A
Second strand synthesis primer: GCCGGTGGCCGCCT	Metabion	N/A
Library amplification Fw: GGAGCTTCTTCTTGGGCTCT	Metabion	N/A
Library amplification Rv: AGCGGAGAAGGGTGAAAGT	Metabion	N/A
NGS primer Fw: ACACTCTTTCCCTACACGACGCTC TTCCGATCTCAGCCACAAAGAAGGAGAGG	Metabion	N/A
NGS primer Rv: GACTGGAGTTCAGACGTGTGCTCTT CCGATCTGTCCTGCCAAACCATACCC	Metabion	N/A
AAV9-Cap-Fw-primer: ACCGCTAGCTTCGATCAACTACGC	Metabion	N/A
Se1-Rv-primer: CCCAACCGGTGGCCGCCTGGGCACC CACAGAACGAACACCATTGCCTGCTT GGCCACTCTGGTGGTTTGTGGCCACTTGTC	Metabion	N/A
Se2-Rv-primer: CCCAACCGGTGGCCGCCTGGGCAAACC GCCCCGGAACACCAGGGCCTGCTTGGC CACTCTGGTGGTTTGTGGCCACTTGTC	Metabion	N/A
AA9-Rv-primer: CCAACCGGTCTGCGCCTGTGCTTGGG CACTCTGGTGGTTTGTGGCCACTTGTC	Metabion	N/A
qPCR-ZsGreen-Fw: GCTCCTTCCTGTTCGAGGAC	Metabion	N/A
qPCR-ZsGreen-Rv: TCGGTCATCTTCTTCATCACG	Metabion	N/A
qPCR-mLmnb2-Fw: CTGAGGGTTGCAGGCAGTAG	Metabion	N/A
qPCR-mLmnb2-Rv: TGTGGACAGACCTGGGTAGG	Metabion	N/A
qPCR-cjLMNB2-Fw: TTCTGGTCTCCATGCCACTC	Metabion	N/A
qPCR-cjLMNB2-Rv: TGGTTCCTGTTGCGTCCTAC	Metabion	N/A
Recombinant DNA		
p9K7 backbone plasmid	This paper	N/A
pXX6	Trepel Martin	Körbelin and Trepel[45]

(*Continued on next page*)

Continued

REAGENT or RESOURCE	SOURCE	IDENTIFIER
piCAP-PHP.eB	Addgene	Cat# 103005
piCAP-Se1-A503W	This paper	N/A
piCAP-Se2-A503W	This paper	N/A
piCAP-AAV9-A503W	This paper	N/A
piCAP-PHP.eB-A503W	This paper	N/A
piCAP-Se1	This paper	N/A
piCAP-Se2	This paper	N/A
piCAP-AAV9	This paper	N/A
pIRES-ZsGreen1	Takara Bio	632478
pCBA-V5-GFP	Broccoli Vania	Luoni et al.[45]
pCBA-ZsGreen	This paper	N/A
pGL4.14-Glo	Promega	Cat# E6691
pCBA-Luc	This paper	N/A
pHelper	Agilent	Cat# 240071
LV-Ef1a-Ly6a	This paper	N/A
LV-Ef1a-Ly6c1	This paper	N/A
LV-Ef1a-Ly6c2	This paper	N/A
pMDLg/pRRE	Addgene	12251
pRSV-Rev	Addgene	12253
pMD2.G	Addgene	12259
pU6-hLY6E-Ef1a-Blast	This paper	N/A
pCAG-Cas9-puro	Broccoli Vania	Luoni et al.[46]
Software and algorithms		
ImageJ	Schneider et al.[47]	https://imagej.nih.gov/ij/
PRISM 8.0	GraphPad	https://www.graphpad.com/features
CRISPOR	Concordet and Haeussler[48]	http://crispor.tefor.net/
TIDE 3.3.0	Brinkman et al.[49]	http://shinyapps.datacurators.nl/tide/

RESOURCE AVAILABILITY

Lead contact

Further information and requests for resources and reagents should be directed to and will be fulfilled by the lead contact, Vania Broccoli (broccoli.vania@hsr.it).

Materials availability

AAV-Se1 and AAV-Se2 sequences are not deposited in public repositories and will be shared by the lead contact upon legitimate request.

Data and code availability

Data: All data reported in this paper will be shared by the lead contact upon request. Code: This paper does not report the original code. Any additional information required to reanalyze the data reported in this paper is available from the lead contact upon request.

METHOD DETAILS

Cell lines

HeLa and 293T cells were purchased from American Type Culture Collection and maintained in Dulbecco Modified Eagle Medium – high glucose containing 10% fetal bovine serum, 1% non-essential amino acids, 1% sodium pyruvate, 1% glutamine, and 1% penicillin/streptomycin. Cells were split every 3–4 days using Trypsin 0.25%.

iPSCs were initially differentiated in Neural Progenitors Cells (NPCs) as described in Iannielli et al.[44] NPCs were, then, dissociated with Accutase and plated on matrigel-coated 6-well plates (3 × 10^5 cells per well) in NPC medium. Two days after, the medium was changed with the differentiation medium containing Neurobasal, 1% Pen/Strep, 1% Glutamine, 1:50 B27, 10 μM SU5402, 8 μM PD0325901, and

10 μM DAPT was added and kept for 3 days. After 3 days, the cells were dissociated with Accutase and plated on poly-L-lysine/laminin/fibronectin (100 μg/mL, 2 μg/mL, 2 μg/mL)-coated 12-well plates (2 × 10^5 cells per well) and 24-well plates (1 × 10^5 cells per well) in neuronal maturation medium supplemented with ROCK inhibitor Y27632 (10 μM) for the first 24 h. Neuronal maturation medium was composed by Neurobasal, 1% Pen/Strep, 1% Glutamine, 1:50 B27, 20 ng/mL human BDNF, 200 μM Ascorbic Acid, 250 μM Dibutyryl cAMP, 10 μM DAPT, 1 μg/μL Laminin. The culture medium was replaced the next day to remove the ROCK inhibitor, and at this stage half of the medium was changed every 2–3 days.

Primary cell cultures

Primary neuronal cultures were prepared at embryonic day 17.5 (E17.5) from mouse embryos. Briefly, cortices were individually dissected, sequentially incubated in trypsin (0.005%, 20 min at 37°C) and DNAse (0.1 mg/mL, 5 min at room temperature) in HBSS (Hank's buffered salt solution without Ca2+ and Mg2+). Cells wand plated on poly-L-lysine coated glasses (2 × 105 cells/cm2) in Neurobasal medium enriched with 0.6% glucose, 0.2%penicillin/streptomycin, 0.25% L-glutamine and 1% B27.

Mice

6-weeks old C57BL/6 and BALBc wild-type mice were purchased from Charles River Laboratories Italia (Calco, Italy). Mice were maintained at San Raffaele Scientific Institute Institutional mouse facility (Milan, Italy) in micro-isolators under sterile conditions and supplied with autoclaved food and water. All procedures were performed according to protocols approved by the internal IACUC and reported to the Italian Ministry of Health according to the European Communities Council Directive 2010/63/EU.

Marmosets

Four adult (3-5years) male common marmosets (Callithrix jacchus), with a body weight between 280 and 330 g, were obtained from the purpose-bred colony of the Biomedical Primate Research Center (BPRC) in the Netherlands. Prior to inclusion in the study, the monkeys underwent elaborate physical examination by the institute's veterinarian, as only healthy monkeys were included. All animals were experimental naive and in good health and free of pathogenic ecto- and endoparasites and common bacteriological infections: Yersinia pestis, Yersinia pseudotuberculosis, Yersinia enterocolitica, Salmonella, Shigella, Aeromonas hydrophilia. They also showed a negative tuberculin reaction. Before the selection of the monkeys a blood sample was taken and tested for lacking any inherent immune response to AAV capsids. The monkeys were pair-housed under conventional conditions in spacious cages with a varying cage environment and were under intensive veterinary care throughout the study. All monkeys were observed for clinical symptoms and the body weight was measured every week. The monkey facility was under controlled conditions of humidity (>60%), temperature (22°C–6°C) and lighting (12 h light/dark cycles from 7 a.m. to 7 p.m.). The animals were daily fed with standard monkey-chow (Special Duit Services, Witham, Essex, UK) in combination with fruits and vegetables and *ad libitum* water supply. This study was performed under project license AVD5020020172687, which was issued by the competent national authorities (Central Committee for Animal Experiments) according to Dutch law, article 10a of the "*Wet op de Dierproeven*". Approval was obtained by the institutional animal welfare body (CCD 008B). All procedures, husbandry, and housing were performed in accordance with the Dutch laws on animal experimentation and the EU Directive 63/2010. The BPRC is accredited by AAALAC International.

In vivo screening of the random AAV9 display peptide library

For the *in vivo* selection, 1 × 10^{11} genomic library particles were injected into the tail vein of BALBc mice. A week later, mice were sacrificed and the complete brain as organ of interest was removed. Total tissue DNA was extracted using the DNeasy Tissue Kit (Qiagen). The random oligonucleotide insertions from the enriched AAV library particles were amplified by PCR using the primers 5′–GGAGCTTCTTCTTGGGCTCT–3′ and 5′– AGCGGAGAAGGGTGAAAGTT–3′. Approximately 20 PCRs with lg template DNA each were set up. The amplicon was purified Wizard SV Gel and PCR Clean-up System (Promega) and was used to produce preselected libraries, using the same procedure described above for the random peptide display library, beginning from SfiI digestion. This procedure was applied to subsequent rounds of selection. Four rounds of selection were performed in $n = 1$ animal each. After each round of selection, ten clones were sequenced. Selected library clones were produced as recombinant AAV vectors for further analysis. In the fourth round of selection not only the on-target tissue but also several off-target organs (liver, spleen, lung, kidney, heart, and muscle) were collected for DNA extraction and PCR extraction as described above.

Next-generation sequencing

Amplicon libraries for Illumina MiSeq next-generation sequencing were amplified for each of four preselected libraries and for all off-target organ of the fourth selection. 1 ng of the amplicon described above was used as template in a PCR reactions using the following pairs of linker primers fw: 5′-ACACTCTTTCCCTACACGACGCTCTTCCGATCTCAGCCACAAAGAAGGAGAGG-3′and rv: 5′- GACTGGAGTTCAGACGTGTGCTCTTCCGATCTGTCCTGCCAAACCATACCC -3′

Which include illumine adapters (underlined sequences). The amplicon was purified submitted at Azenta for Amplicon EZ sequencing. Each sample was sequenced with a depth of at least 500 000–reads. Data analysis was performed by a custom script.

Computational analysis

FASTQ reads were quality checked and trimmed. Random oligonucleotide sequences were identified by searching sequence reads for exact matches of the two sequences CCAAGCAGGC and GCCCAGGCGG, which flank the random insert within the AAV9 cap sequence. The obtained sequences were sorted into clusters of identical sequences and subsequently different filters were applied to remove possible artifacts. First, sequences whose length diverged from the expected length were not considered for further analysis. To remove sequences containing sequencing errors, it was then checked for every sequence if it was at least 100 times less abundant than any other sequence. If the Levenshtein distance between two such sequences was 1, we excluded the less abundant sequence from further analysis. The remaining sequences were translated into peptides. During this process, only sequences were counted that were composed of nucleotide trimers matching the coding scheme of the oligonucleotide synthesis (Figure 1). Downstream statistics and Plot drawing were performed with R script.

Generation of packaging plasmids and gene transfer vectors

Plasmid encoding the modified AAV capsid of interest were subcloned into iCAP-PHP.eB (Addgene). The mutated version of Se1 and Se2 were generated using as donor sequence the clones derived from the third round of selection which contained the heptapeptide at position 589 and the W503A mutation (VP1 numbering). The restriction fragment SapI-AfeI purified from the Se1 and Se2 clones was cloned into the vector iCAP-PHP.eB digested NheI-AfeI and ligated with a second restriction fragment (NheI-SapI) extracted from the same vector, thus originating the plasmids for the production of AAV-Se1-A503 and AAV-Se2-A503 vectors. Conversely wild-type plasmids coding for W in position 503 of VP1 (AAV-Se1, AAV-Se2 and AAV9) were produced using PCR amplification of the CAP cistron of tTA-iCAP-PHP.eB using a common fw primer 5′- ACC**GCTAGC**TTCGATCAACTACGC-3′ and reverse primers containing the desired heptapeptide ant position 589 (underlined) or the native sequence of AAV9 flanked by an AgeI site (bold):

Se1-Rv:

5′CCCA**ACCGGT**GGCCGCCTGGGCACCCACAGAACGAACACCATTGCCTGCTTGGCCACTCTGGTGGTTTGTGGCCACTTGTC -3′;

Se2-Rv:

5′CCCA**ACCGGT**GGCCGCCTGGGCAAACCGCCCCGGAACACCAGGGCCTGCTTGGCCACTCTGGTGGTTTGTGGCCACTTGTC-3′;

AAV9-Rv: 5′-CCAA**CCGGTC**TGCGCCTGTGCTTGGGCACTCTGGTGGTTTGTGGCCACTTGTC-3′.

For AAV9-A503 the same oligos for AAV9 were used but as template AAV-Se2-A503 was used.

Amplicons were restriction digested with NheI and AgeI as well as iCAP-PHP.eB vector and cloned. The coding sequences for ZsGreen (pIRES2-ZsGreen1, Takara Bio) and Luciferase (*luc2*, pGL4.14-Glo, Promega) were cloned into a ssAAV-CBA vector (Luoni et al., 2020).

AAV virus production and purification

AAV replication-incompetent, recombinant viral particles were produced 293T cells, by polyethylenimine (PEI) co-transfection of three different plasmids: the gene transfer vector, the packaging plasmid (see above) and pHelper (Agilent) for the three adenoviral helper genes. The cells and supernatant were harvested at 120 h. Cells were lysed in hypertonic buffer (40 mM Tris, 500 mM NaCl, 2 mM $MgCl_2$, pH = 8) containing 100 U/ml Salt Active Nuclease (SAN, Arcticzymes) for 1 h at 37°C, whereas the viral particles present in the supernatant were concentrated with 8% PEG8000 (Polyethylene glycol 8000, Sigma-Aldrich) by precipitation (4000g, 20 min). In order to clarify the lysate, cellular debris were separated by centrifugation (4000g, 30 min). The viral phase was isolated by iodixanol step gradient (15%, 25%, 40%, 60% Optiprep, Sigma-Aldrich) in the 40% fraction and concentrated in PBS (Phosphate Buffer Saline) with 100K cut-off concentrator (Amicon Ultra15, MERCK-Millipore). Virus titers were determined using AAVpro Titration Kit Ver2 (TaKaRa Bio).

Lentivirus virus production and purification

GPI coding sequences (Ly6a: NM_001271416; Ly6c1: NM_001252055; Ly6c2: NM_001099217) were gene synthetized (Azenta) with flanking restriction sites apt for sub-cloning into the LV-Ef1a backbone.[45] Lentiviral replication-incompetent, VSVg-coated lentiviral particles were packaged in 293T cells.[42] Cells were transfected with 30 μg of vector and packaging constructs, according to a conventional $CaCl_2$ transfection protocol. After 30 h, medium was collected, filtered through 0.44 μm cellulose acetate and centrifuged at 20000 rpm for 2 h at 20°C in order to concentrate the virus.

In vivo administration of AAV vectors in mice and tissue collection

Vascular injection was performed in a restrainer that positioned the tail in a heated groove. The tail was swabbed with alcohol and then injected intravenously with a viral concentration (1×10^{12} to vg/mL) in a total volume of 100 μL of recombinant AAV particles in PBS. C57BL/6 and BALBc mice, independently of sex, were randomized in groups and injected in the tail vein between 30 and 40 days of age. Following injection, all mice were monitored for adverse effect and two weeks after infection were sacrificed and tissues harvested. Briefly, mice were anesthetized with ketamine/xylazine and transcardially perfused with 0.1 M phosphate buffer (PB) at room temperature (RT) at pH 7.4. Upon this treatment brain and liver were collected. Brain hemispheres were separated: one-half was post-fixed in 4% paraformaldehyde (PFA) for two days and then soaked in cryoprotective solution (30% sucrose in PBS) for immunofluorescence analysis, the other half was further sectioned in different areas (cortex and cerebellum) quick-frozen on dry-ice for Western blot, RNA and DNA extraction. Liver specimens were collected similarly.

Testing basal immunity to AAV capsids in NHPs

Sera of six untreated animals were collected for neutralizing antibodies detection: HeLa cells were plated in 96-well plate (6×10^4 cells/cm^2). The day after Monkey sera and Pooled Human Sera (PHS, Dunn Labortechnik GmbH) were heat inactivated (56°C, 30′), filtered (0.22 μm) and serially diluted in semi-log fashion. Each dilution was supplemented with AAV9-Luciferase (1×10^8 vg/well) and negative (no virus) and positive controls (no serum) were sat. After incubation (1 h, 37°C) these solutions were added to HeLa Cells and incubated overnight (37°C, 5% CO_2). The day after the plates were pre-cooled (RT, 15′) supplemented with luciferase substrate (Bright Glo Luciferase Assay System, Promega) incubated (RT, 30′) and luminescence was red with Victor^3 microplate reader (PerkinElmer).

In vivo administration of AAV vectors in marmosets and tissue collection

Clinical chemistry and hematological parameters were checked in blood samples for abnormalities before the start of the study, and for possible aversive effects of the treatment at the end of the study. AAVG, AAV-Se1 or -Se2 was administered intravenous (femoral vein) in a single dose (3×10^{13} vg) of in a volume of 1 mL under sedation with 12 mg/kg alfaxan IM (Vetoquinol, 's-Hertogenbosch, The Netherlands. After injection, the animals were closely monitored during a 3-h recover period. Thereafter, the monkeys were daily observed for possible clinical signs like immobility, apathy, loss of appetite, and changes in movement. The body weight of the monkeys was measured once a week. During the study, the monkeys stayed in pairs together in their own home cage. Three weeks after the injection the monkeys were euthanized for collection of blood and tissues. Just before euthanasia, the monkeys were weighed and 2 mL serum for clinical chemistry, 2 mL plasma for hematology, and 2 mL EDTA blood for further analysis, was withdrawn from the femoral vein. Euthanasia was induced with Alfaxan 10 mg/kg + Ketamine 10 mg/kg IM. Immediately thereafter, the brains and other organs were removed in the section room. The whole brain was taken and weighed. The brain was cut into two hemispheres (including the brain stem). One hemisphere was stored in 4% formalin for 48 h. The other hemisphere was cut into different brain areas (cerebellum, pons, medulla, hippocampus, striatum, thalamus, temporal cortex, frontal cortex, visual cortex, putamen, and caudate nucleus) and snap frozen in liquid nitrogen and stored at −80°C. All the remaining parts of the brain were also stored at −80°C for qPCR analysis. From the other organs (kidney, liver, heart, spleen, lung, muscle hamstring, terminal ileum and colon) two parts were collected and stored in 4% formalin (48 h) or frozen in liquid nitrogen and stored at −80°C.

Immunofluorescence

Tissues were sectioned using cryostat after optimal cutting temperature compound (OCT) embedding in dry ice. Free-floating 50μm-thick coronal sections were rinsed in PBS and were incubated with 10% donkey serum and 3% Triton X-100 for 1 h at RT to saturate the unspecific binding site before the overnight incubation at 4°C with the primary antibody (diluted in the blocking solution). Fixed cells and tissues were washed with PBS (3×) and incubated with 10% donkey serum and Triton X-100 (3% for tissues and 1% for cells) for 1 h at RT to saturate the unspecific binding site before the overnight incubation at 4°C with the primary antibody. Upon wash with PBS (3×), cells and tissues were incubated for 1 h, at RT in blocking solution with DAPI and with Alexa Fluor 488 and Alexa Fluor 594 anti-rabbit, anti-mouse or anti-rat secondary antibodies (1:1000, ThermoFisher Scientific). After PBS washes (3×), cells and tissues were mounted with fluorescent mounting medium (Dako). When immunohistochemistry was preferable, the biotinylated secondary antibody was coupled with avidin/biotinylated enzyme complex for 1 h and then revealed with the DAB solution (Vector Laboratories). Cell and tissue were stained with the following primary antibody: rabbit anti-ZsGreen (1:500; Takara), rabbit anti-NeuN (1:500; Merck), rabbit anti-Sox9 (1:500; Merck), rabbit anti-Calbindin (1:500; Swant), rat anti-CD-31 (1:500; BD biosciences), chicken anti-MAP2 (1:500; Abcam), chicken anti-Iba1(1:500, SYSY), rabbit anti-Olig2 (1:300, Merck).

Acquisition and quantification of immunofluorescent images

Brain and liver low magnification images were captured with a Nikon Eclipse 600 fluorescent microscope with using a 4× magnification. Each captured field was overlapping with the adjacent one, in order to allow reconstruction of the entire organ image using ImageJ software. Cell culture fluorescence was image using the same microscope. High magnification images of mouse and marmoset brains were acquired with Leica TCS SP8 Laser Scanning Confocal microscope using ×40 magnification lens (HCPL APO CS2 40x/1.30 oil) over five 50-μm-thick sections. Acquisition parameters were as follow: Resolution: 1024 × 1024 pixel (291 × 291 nM); Gray value: 8 bit; Scan speed: 100 Hz; Pin hole: 6.5 nm, Airy Unit: 1; lasers set-up: blue channel: excitation: 405 nm, intensity 1%, detector: 420–480 nm, green channel: excitation: 488 nm, intensity 10%, detector: 505–550 nm, red channel: excitation: 552 nm, intensity 10%, detector: 565–620 nm. Microscope settings were replicated identically thought all the specimens, directly compared in the same figure. For the quantification of transduced cells in the cortex and cerebellum, we acquired 3 images per 3 fields. All the images were processed by using ImageJ. To assure the unbiased quantification of the fluorescence images we blinded-assigned a fixed signal threshold for each experimental setup thus, we generated a macro for the automated image analysis. In mice, the quantification of colocalizing cells or the Iba1 signal intensity was represented as the median of all the images for each field, analyzing three independent animals. In marmosets, due to the limited number of animals, the three fields were analyzed separately. Here, the median is representative of the images for a single field.

Determination of vector copy numbers by qPCR

Total DNA was isolated from animal tissues (cortex, cerebellum, liver, heart, muscle) using the Qiagen DNeasy Blood & Tissue Kits (QIAGEN). The quantification of vector transgene expression was calculated by qRT-PCR relative to the ZsGreen transgene using the following primers: 5′-GCTCCTTCCTGTTCGAGGAC-3′and 5′- TCGGTCATCTTCTTCATCACG-3′. The DNA levels were normalized against an amplicon from a single-copy mouse gene: in murine samples: murine Lmnb2, amplified from genomic DNA using 5′-CTGAGGGTTGCAGGCAGTAG-3′and 5′-TGTGGACAGACCTGGGTAGG-3′; in simian samples: Callithrix jacchus LMNB2 amplified from genomic DNA using 5′-TTCTGGT CTCCATGCCACTC-3′and 5′-TGGTTCCTGTTGCGTCCTAC-3′. Depending on the control samples Normalization was applied.

CRISPR/Cas9 gene editing in HeLa cells

We used the program CRISPOR (http://crispor.tefor.net) to design sgRNAs on exon 3 of the human LY6E gene (Gene ID: 4061). Efficiency of three different sgRNAs was compared in HEK293 cells and we selected sgRNA#1 (5′-agaaggcgtcaatgttggtg-3′) for its high activity of INDEL rate using the T7 Endonuclease I assay. Then, HeLa cells were co-transfected with the vectors U6-sgRNA#1-EF1α-Blast and the pCAG-Cas9-Puro using the Lipofectamine Transfection Reagent (Invitrogen).[50] Co-transfected colonies were then selected by the combination of puromycin (1 μg/mL) and blasticidin (10 μg/mL) and then isolated through single colony picking. Finally, resistant cell clones were assessed by TIDE analysis followed by Sanger sequencing for isolating either clones with the targeted genomic modification in the LY6E gene or clones with the unmodified LY6E gene (control cells).

Transduction assay in neuronal and cell cultures

Primary neuronal cultures: Viral particles were directly added to cultured neurons 3 days after seeding, with a final concentration 1×10^{10} vg/mL. All the analysis ware conducted one week after the infection.

iPSCs: Viral particles were directly added to cultured neurons after six weeks of differentiation, with a final concentration 1×10^{10} vg/mL. All the analysis ware conducted one week after the infection.

HeLa cells: For transduction assay cells were plated (2×10^5 cells/cm^2) and infected at the first day *in vitro* (DIV1) with lentiviral vectors expressing GPI protein. At DIV 3 cells were replated (2×10^5 cells/cm^2) and infected with different AAV recombinant virus carrying ZsGreen transgene (4×10^9 vg/mL) and finally at DIV6 the analysis was performed.

All Cultures were fixed for immunofluorescence staining (4% PFA, 4°C, 30′) or for FACS analysis (4% PFA, 4°C, 10′). In the former case cell were washed, resuspended (PBS, 2% FBS) and filtered (70 mm), and ZsGreen fluorescence was analyzed by CytoflexS.

QUANTIFICATION AND STATISTICAL ANALYSIS

Values are expressed as mean ± standard deviation as indicated. All statistical analysis was carried out in Prism 8.0 (GraphPad), using one-way ANOVA. P-values below 0.05 were considered significant. In multi-group comparisons, multiple testing correction for pairwise tests among groups was applied using Tukey's post hoc analysis.